Title
Estuary-enhanced upwelling of marine nutrients fuels coastal productivity in the U.S. Pacific Northwest

Authors
Davis, KA
Banas, NS
Giddings, SN
et al.

Publication Date
2015

DOI
10.1002/2014JC010248

Peer reviewed

AGU PUBLICATIONS

JGR

Journal of Geophysical Research: Oceans

RESEARCH ARTICLE

10.1002/2014JC010248

Estuary-enhanced upwelling of marine nutrients fuels coastal productivity in the U.S. Pacific Northwest

Kristen A. Davis[1], Neil S. Banas[2], Sarah N. Giddings[3], Samantha A. Siedlecki[2], Parker MacCready[4], Evelyn J. Lessard[4], Raphael M. Kudela[5], and Barbara M. Hickey[4]

[1]Department of Civil and Environmental Engineering, University of California, Irvine, California, USA, [2]Joint Institute for the Study of the Atmosphere and Ocean, University of Washington, Seattle, Washington, USA, [3]Scripps Institution of Oceanography, University of California, San Diego, La Jolla, California, USA, [4]School of Oceanography, University of Washington, Seattle, Washington, USA, [5]Ocean Sciences Department, University of California, Santa Cruz, California, USA

Key Points:
- Outflow from the SJDF is a critical source of nitrogen to coastal PNW waters
- *N* exported from the SJDF is of ocean origin (98%) during upwelling season
- A physical-biological model predicts *N* and *P* distribution in PNW waters

Correspondence to:
K. A. Davis,
davis@uci.edu

Citation:
Davis, K. A., N. S. Banas, S. N. Giddings, S. A. Siedlecki, P. MacCready, E. J. Lessard, R. M. Kudela, and B. M. Hickey (2014), Estuary-enhanced upwelling of marine nutrients fuels coastal productivity in the U.S. Pacific Northwest, *J. Geophys. Res. Oceans*, *119*, 8778–8799, doi:10.1002/2014JC010248.

Received 14 JUN 2014
Accepted 15 NOV 2014
Accepted article online 22 NOV 2014
Published online 22 DEC 2014

Abstract The Pacific Northwest (PNW) shelf is the most biologically productive region in the California Current System. A coupled physical-biogeochemical model is used to investigate the influence of freshwater inputs on the productivity of PNW shelf waters using realistic hindcasts and model experiments that omit outflow from the Columbia River and Strait of Juan de Fuca (outlet for the Salish Sea estuary). Outflow from the Strait represents a critical source of nitrogen to the PNW shelf-accounting for almost half of the primary productivity on the Vancouver Island shelf, a third of productivity on the Washington shelf, and a fifth of productivity on the Oregon shelf during the upwelling season. The Columbia River has regional effects on the redistribution of phytoplankton, but does not affect PNW productivity as strongly as does the Salish Sea. A regional nutrient budget shows that nitrogen exiting the Strait is almost entirely (98%) of ocean-origin—upwelled into the Strait at depth, mixed into surface waters by tidal mixing, and returned to the coastal ocean. From the standpoint of nitrogen availability in the coastal euphotic zone, the estuarine circulation driven by freshwater inputs to the Salish Sea is more important than the supply of terrigenous nitrogen by rivers. Nitrogen-rich surface waters exiting the Strait follow two primary pathways—to the northwest in the Vancouver Island Coastal Current and southward toward the Washington and Oregon shelves. Nitrogen flux from the Juan de Fuca Strait and Eddy Region to these shelves is comparable to flux from local wind-driven upwelling.

1. Introduction

Along the west coast of the United States and within the California Current System (CCS), alongshore winds drive the upwelling of dense, nutrient-rich water onto the continental shelf in summer [*Smith*, 1974; *Huyer*, 1983]. This upwelling fuels the growth of phytoplankton and higher trophic levels [*Small and Menzies*, 1981; *Hales et al*., 2005; *Ware and Thomson*, 2005]. However, this simple model of wind-driven biological productivity does not adequately describe the northern CCS, where the region of highest primary productivity (coastal waters of Washington and southern British Columbia) is not colocated with the highest magnitude of upwelling-favorable alongshore winds (northern California coast) [*Ware and Thomson*, 2005]. This apparent paradox was addressed by *Hickey and Banas* [2008] who discuss mechanisms that can contribute to elevated productivity in the northern region of the CCS. First, the Pacific Northwest (PNW) coastal regions have a high density of shelf-break canyons, which enhance upwelling [*Allen and Hickey*, 2010; *Connolly and Hickey*, 2014]. Second, the Washington and Oregon continental shelves are generally wider than the California shelf, promoting retention of upwelled nutrients and the resultant phytoplankton blooms as opposed to rapid export offshore in jets, as commonly happens farther south in the CCS [*Strub et al*., 1991]. Third, energy from coastal trapped waves generated in areas with greater wind stress (northern California) contributes to upwelling in the northern CCS [*Connolly and Hickey*, 2014; *Hickey et al*., 2006]. Finally, the PNW coastal region receives greater input of freshwater, which plays a complex role in coastal productivity and is the subject of this paper.

In the Pacific Northwest, coastal waters are strongly influenced by freshwater input from the Columbia River and the rivers of the Salish Sea (Fraser River and other rivers flowing into the Strait of Georgia, Puget Sound, or the Strait of Juan de Fuca). The Columbia River plume and its effect on local biophysical dynamics has

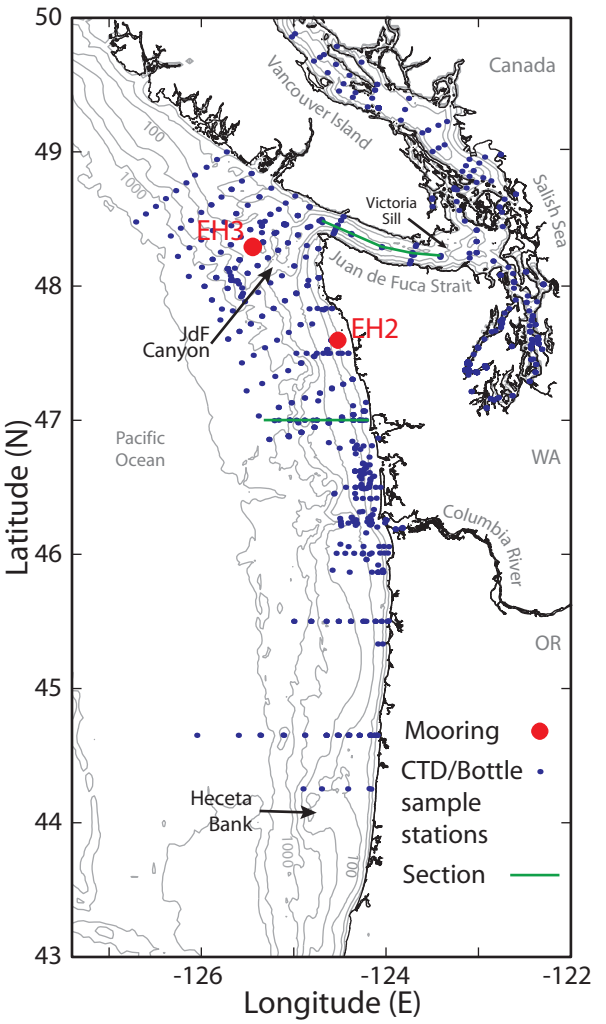

Figure 1. Map of Cascadia model domain with locations of observational data. Bathymetry contours are at 30, 50, 100, 180, 500, 1000, 2000, 3000, and 4000 m depth.

been the subject of many studies. Observations by *Lohan and Bruland* [2006] and modeling work by *MacCready et al.* [2009] emphasize the importance of tidal and wind mixing processes in the near-field Columbia River plume to the distribution of nitrate and iron in shelf waters. In a modeling study of the Columbia River region, *Banas et al.* [2009a] found that the presence of the Columbia River plume had the dual effect of shifting primary production to deeper water and increasing retention time and planktonic community age on the shelf. Simulations by *Giddings et al.* [2014] find that the plume plays a major role in the transport of harmful algal blooms (HABs) to the Washington coast.

The 20 km wide Strait of Juan de Fuca (Figure 1) is the primary connection between the Salish Sea (composed of Puget Sound, the Strait of Georgia and the Strait of Juan de Fuca) and the ocean. The Fraser River accounts for approximately 73% of the freshwater in this outflow [*Waldichuk*, 1957; *Johannessen et al.*, 2003]. Estuarine circulation drives the exchange, with fresher water flowing seaward near the surface and a deep return flow carrying dense, nutrient-rich ocean water landward [*Herlinveaux and Tully*, 1961; *Masson*, 2006]. Salinity gradients and gravitational convection within the Strait are determined by tidal mixing over shallow sills [*Griffin and LeBlond*, 1990], the seasonal cycle of freshwater discharge [*Hansen and Rattray*, 1966], and local winds [*Holbrook et al.*, 1980].

Several studies have suggested that the upwelling of ocean-derived nutrients into the Strait can strongly influence biogeochemical cycles and the timing of spring blooms within the estuary [*Allen and Wolfe*, 2013; *Khangaonkar et al.*, 2012; *Mackas and Harrison*, 1997]. Circulation within the Strait also impacts the coastal regions outside the estuary. Observational work by *Crawford and Dewey* [1989] implicates outflow from the Strait as the primary source of nutrients to the Vancouver Island shelf. The Juan de Fuca Eddy, which forms seasonally just seaward of the mouth of the Strait (Figure 1), has been shown by drifter and modeling studies to be a strongly retentive feature [*MacFadyen and Hickey*, 2010; *MacFadyen et al.*, 2005] and a "hot spot" for the harmful algal species *Pseudo-nitzschia* and the toxin domoic acid [*Trainer et al.*, 2009]. The transport of surface waters from the Juan de Fuca Strait and Eddy region has implications for harmful algal blooms, oxygen levels, and the biological productivity of the Pacific Northwest coastal regions [*Crawford and Peña*, 2013; *MacFadyen et al.*, 2008] (*Siedlecki et al.*, 2014).

While previous observational and modeling studies have examined smaller-scale dynamics of the Columbia River plume and Juan de Fuca Strait and Eddy, this study takes a holistic approach and employs a coupled physical-biological numerical model of the Oregon-Washington-British Columbia shelves along with the

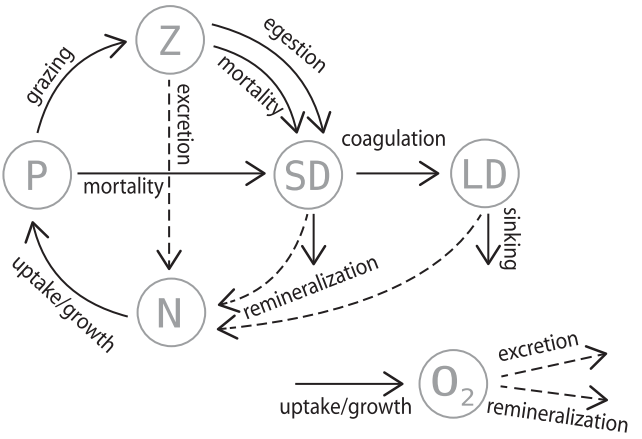

Figure 2. Schematic of the Cascadia ecosystem model. Circles represent pools of nitrogen in the form of dissolved inorganic nitrogen (*N*), phytoplankton (*P*), zooplankton (*Z*), small detritus (*SD*), large detritus (*LD*), and oxygen (O_2). Arrows represent fluxes of nitrogen between the pools.

Columbia estuary and (for physics only) the inland waters of the Salish Sea. By resolving the Salish Sea, we achieve a realistic exchange flow within the Strait and also predict the dynamics of multiple freshwater plume interactions [*Giddings et al*., 2014; *Hickey et al*., 2009; *Sutherland et al*., 2011]. The hydrodynamic and ecosystem models are described in section 2 and a detailed comparison of ecosystem model output with observational data, primarily collected during Ecology and Oceanography of Harmful Algal Blooms-Pacific Northwest (ECOHAB-PNW) [*MacFadyen et al*., 2008] and River Influences in Shelf Ecosystems (RISE) [*Hickey et al*., 2010] experiments is made in section 3.

We use this model to quantify the role of freshwater inputs and estuarine circulation within the Strait in maintaining the high levels of productivity and biomass observed along the PNW shelf. In section 4, we use 3 years of realistic hindcasts together with experimental simulations in which outflow from the Columbia River and the Salish Sea are removed to isolate the influence of these freshwater sources on biological productivity of the PNW shelf. Additionally, a budget for total nitrogen in the Juan de Fuca Strait and Eddy region is used to describe regional patterns in nitrogen transport. In section 5, we discuss the sources and fate of nitrogen exiting the Strait of Juan de Fuca and consider physical mechanisms that modify the flux of nitrogen to the PNW coastal euphotic zone. Our findings are summarized in section 6.

2. Methods

2.1. Circulation Model

The circulation model is an implementation of the Regional Ocean Modeling System (ROMS, Rutgers version 3.5) [*Haidvogel et al*., 2000], a free-surface, hydrostatic, primitive equation model. A detailed description of the particular configuration of ROMS used in this study (the University of Washington Coastal Modeling Group "Cascadia" model) along with a comprehensive skill assessment of the physical model can be found in *Giddings et al*. [2014] and a similar configuration in *Sutherland et al*. [2011]. The model domain, shown in Figure 1, encompasses coastal Washington, northern Oregon, and southern Vancouver Island, including the Salish Sea, Columbia River plume region, and Heceta Bank. Horizontal resolution is 1.5 km along coastal Washington and increases to 4 km at the boundaries. The model uses 40 vertical, terrain-following layers (*s*-coordinates) and vertical resolution is enhanced near the sea surface and at the bed. The model utilizes the k-ε version of the Generic Length Scale formulation for turbulence closure [*Umlauf and Burchard*, 2003] with Canuto-A stability functions [*Canuto et al*., 2001].

2.2. Ecosystem Model

The ecosystem model used in this study (Figure 2) is based on one developed by *Banas et al*. [2009a] for the Columbia River plume region. The *Banas et al*. [2009a] model tracks nitrogen in four pools: dissolved nutrients (*N*), phytoplankton (*P*), microzooplankton (*Z*), and detritus (*D*). For this study, a large detritus pool was added to improve the vertical profile of dissolved nutrients in waters on the continental shelf and slope (*Siedlecki et al*., 2014), and so we will refer to small detritus (*SD*) and large detritus (*LD*). The use of a nitrogen-based model is motivated by *Bruland et al*. [2008] and *Kudela and Peterson* [2009], which find phytoplankton growth on the Washington and Oregon coasts to be primarily nitrogen-limited. The model nutrient pool, *N*, includes all forms of dissolved inorganic nitrogen (nitrate, nitrite, ammonium, and others); "total nitrogen" refers to the complete sum $N + P + Z + SD + LD$. The model equations are as follows:

Table 1. Ecosystem Parameters

	Description	Value	Source
μ_0	Maximum instantaneous growth rate	1.7 d^{-1}	RISE/ECOHAB observations: dilution experiments, 2003–2005 ($n = 101$)
att_{sw}	Light attenuation by seawater	0.05–0.0065 (S−32) m^{-1} (where S = salinity)	RISE observations: PAR data from CTD casts, 2004–2005 ($n = 43$)
att_p	Light attenuation by phytoplankton	0.03 m^{-1}	RISE observations: PAR data from CTD casts, 2004–2005 ($n = 43$)
α	Initial slope of the growth-light curve	0.07 (W m^{-2})$^{-1}$$d^{-1}$	RISE/ECOHAB observations: photosynthesis-Irradiance curves from deckboard incubations, 2004–2006 ($n = 55$)
k_s	Minimum half-saturation for Nutrient uptake (*Optimal Uptake Model*)	0.1	RISE/ECOHAB observations: dilution experiments, 2003–2005 ($n = 101$)
m	Non-grazing phytoplankton Mortality	0.1 d^{-1}	A Priori
Chl:N	Chlorophyll-to-nitrogen ratio	2.5 mg Chl (mmol N)$^{-1}$	RISE observations: CTDs 2004–2005 ($n = 121$)
I_0	Maximum ingestion rate	4.8 d^{-1}	RISE/ECOHAB observations: dilution experiments near growth-grazing equilibrium ($n = 9$)
ξ	Zooplankton mortality	2.0 d^{-1} (μM N)$^{-1}$	RISE/ECOHAB observations: dilution experiments near growth-grazing equilibrium (n=9)
K_s	Half-saturation for ingestion	3 μM N	Lab studies: average for ~60 microzooplankton and mesozooplankton spp. [*Hansen et al.*, 1997]
ε	Gross growth efficiency of Zooplankton	0.3	Lab studies: average for ~60 microzooplankton and mesozooplankton spp. [*Hansen et al.*, 1997]
f_{egest}	Fraction of losses egested	0.5	A Priori
r	Remineralization rate	0.1 d^{-1}	Th based flux measurements at HOT [*Dunne et al.*, 1997] Roller tank experiments on diatoms [*Groussart and Ploug*, 2001]
w_{LD}	Sinking rate for large detritus	80 m d^{-1}	A Priori
w_{SD}	Sinking rate for small detritus	8 m d^{-1}	A Priori
χ	Loss of nitrate to the sediments	1.2 mmol NO_3 m^{-2} d^{-1}	Observations from the Oregon coast of a constant loss to the sediments from 80–1000 m [*Hartnett and Devol*, 2003]
τ	Detrital coagulation rate	0.05 (mmol N m^{-3})$^{-1}$ d^{-1}	A Priori

$$\frac{\partial P}{\partial t} = \mu_i(E,N)P - I(P)Z - mP + advection + diffusion \tag{1a}$$

$$\frac{\partial Z}{\partial t} = \varepsilon I(P)Z - \xi Z^2 + advection + diffusion \tag{1b}$$

$$\frac{\partial SD}{\partial t} = (1-\varepsilon)f_{egest}I(P)Z + mP + \xi Z^2 - rSD - \tau(SD)^2 - w_{SD}\frac{\partial SD}{\partial z} + advection + diffusion \tag{1c}$$

$$\frac{\partial LD}{\partial t} = \tau(SD)^2 - rLD - w_{LD}\frac{\partial LD}{\partial z} + advection + diffusion \tag{1d}$$

$$\begin{aligned}\frac{\partial N}{\partial t} &= -\mu_i(E,N)P + (1-\varepsilon)(1-f_{egest})I(P)Z \\ &+ rSD + rLD - F^{benthic}_{denitr} - F^{wc}_{denitr} + advection + diffusion\end{aligned} \tag{1e}$$

Model parameter definitions and units are given in Table 1. Phytoplankton growth rate (μ_i) is limited by light availability and the uptake of nutrients (equation (2)). The hyperbolic Michaelis-Menten equation is often used to describe the uptake rate of nutrients as a function of their ambient concentration [*Droop*, 1974; *Dugdale*, 1967], and while it performs well in short-term experiments it has less skill predicting growth rates over a wide range of nutrient concentrations [*Gotham and Rhee*, 1981]. We use the alternate formulation presented by *Smith et al.* [2009] which incorporates a physiological trade-off between the efficiency of nutrient encounter at the cell surface and the maximum rate of nutrient assimilation. Assuming optimization of intracellular resources allows for differentiation of the half-saturation for nutrient uptake (k_s) between the high-nutrient shelf conditions and low-nutrient open ocean conditions:

$$\mu_i(E,N) = \mu_0 \frac{N}{k_{s,app}+N} \frac{\alpha E}{\sqrt{\mu_0^2+\alpha^2E^2}} \tag{2}$$

where the apparent half-saturation

$$k_{s,app} = k_s + 2\sqrt{k_s N}\ .$$

Photosynthetically available radiation (PAR or E in equation (3)) at depth z is a function of light attenuation due to the optical properties of seawater and self-shading by phytoplankton. Light attenuation parameters (att_{sw} and att_P) are derived from PAR, chlorophyll *a*, and salinity measurements from 43 CTD casts taken between 45.5°N and 47.5°N during the 2004–2005 RISE cruises. A salinity-dependence in the formulation

for att_{sw} (see Table 1) is used to express the gradient in optical properties across the water types within our domain (river plume, estuarine, open ocean) as described by the CTD PAR measurements.

$$E(z) = E_{surface}\exp\left(att_{sw}(S)z + att_P \int_z^{surface} P\left(z'\right)dz'\right) \quad (3)$$

Following [*Banas et al*., 2009a], the functional form for zooplankton ingestion $I(P)$ (in equation (1b)) includes a quadratic prey saturation response:

$$I(P) = I_0 \frac{P^2}{K_s^2 + P^2}, \quad (4)$$

where K_s is a half saturation coefficient and total zooplankton ingestion is divided into zooplankton net growth, excretion, and egestion using two parameters, ε and f_{egest} (Figure 2).

The parameterization of detrital processes was designed to reproduce observed vertical profiles of nutrients and oxygen, as described by *Siedlecki et al*. [2014]. The best agreement was found with the addition of a second detrital pool, where large detritus (*LD*) is formed from the coagulation of small detritus (*SD*) at the rate of 0.5 mmol N m^{-3} d^{-1}, sinking rates are 8 m d^{-1} (*SD*) and 80 m d^{-1} (*LD*), and where all detritus is respired and returns to the dissolved nutrient pool at the bed: that is, there is assumed to be no burial of organic matter. A loss of nitrogen can occur via either benthic or water-column denitrification (equation (1e)) (see *Siedlecki et al*., 2014, for further discussion). The benthic denitrification flux, applied to the deepest grid layer only, is

$$F_{denitr}^{benthic}|_{z=-H} = \min\left(\frac{\chi}{\Delta z}, w_{SD}\frac{\partial SD}{\partial z}\bigg|_{z=-H} + w_{LD}\frac{\partial LD}{\partial z}\bigg|_{z=-H}\right) \quad (5)$$

where χ is 1.2 mmol N m^{-2} d^{-1} [*Hartnett and Devol*, 2003], Δz the grid layer depth, and the vertical gradients in detrital concentration are dynamically calculated at each time step across the bottom two grid cells. This formulation limits benthic denitrification to be no greater than the current flux of organic matter to the benthos, a threshold that is typically reached around the 1000 m isobath in our model. Water-column denitrification is formulated so that when dissolved oxygen concentration O_2 (see *Siedlecki et al*., 2014) is too low to support the bacterial respiration required for the remineralization flux specified in equations (1c) and (1d), the *N* pool is drawn down instead:

$$F_{denitr}^{wc} = \frac{1}{c_{O:N}} max\left(c_{O:N}r(SD+LD) - \frac{O_2}{\Delta t}, 0\right) \quad (6)$$

where Δt is the model time step and $c_{O:N}$ = 108:16 mol:mol.

2.3. Boundary Conditions

Initial conditions for ocean temperature, salinity, subtidal velocities, and sea surface height are interpolated to the grid from the global Navy Coastal Ocean Model (NCOM) [*Barron et al*., 2006]. NCOM does not extend into Puget Sound and the Strait of Georgia, so initial conditions for temperature and salinity in these regions were derived from an extension of NCOM values with salinity gradients applied near river mouths. At the southern and western open boundaries the physical fields are relaxed to NCOM values over a six grid point region. The northern boundary of the Strait of Georgia is closed, but experimental runs with an open boundary at that location did not produce significantly different results. Three-hourly winds and atmospheric forcing are taken from the 4 km Northwest Regional Modeling Consortium MM5 regional forecast model [*Mass et al*., 2003] and tidal forcing is applied to open boundary conditions using eight tidal constituents from the TPXO7.2 global tidal model [*Egbert and Erofeeva*, 2002].

NCOM supplies the physical water properties entering the domain at the western and southern boundaries, but chemical and biological tracers (N, P, Z, SD, LD, and O_2) obey a zero horizontal gradient on the open ocean boundaries. Initial conditions for dissolved nutrients (*N*) are imposed as a piecewise linear fit to salinity based on regressions using all available ECOHAB-PNW and RISE bottle salinity and nitrate samples (Table 2). A correction for the low bias in NCOM-Global salinity was included in the nutrient boundary condition derivation. Since available bottle data did not capture deep water sources (less than 2% of RISE and

Table 2. Salinity-Nitrogen Fit for Nutrient Boundary Condition

Salinity Class, S	N (μM)
<31.9	$= 0$
31.9–33	$= 20.15S–642.8$
33–33.82	$= 9.59S–294.3$
33.82–34.25	$= 34.83S–1148$
34.25–34.3	$= 45$
>34.3	$= -37.3S + 1324$
Salish Sea	$= 3.26S–76.44$

ECOHAB-PNW bottle samples were collected deeper than 300 m), the nearest available World Ocean Circulation Experiment (WOCE) data (between 30°N and 32°N and −117°E and −120°E) were used to constrain the deep salinity-nitrate relationship [*WOCE Data Products Committee*, 2002]. Initial conditions for N in the Salish Sea (from −123.5°E in the Strait) were derived from 93 CTD casts over the Victoria Sill and in the eastern Strait of Juan de Fuca (−123°E to 123.4°E, 48.2°N–48.4°N) from 1998 to 2000 [sources: *Masson and Cummins*, 2004, Puget Sound Regional Synthesis Model (PRISM), and ECOHAB-PNW cruises].

Freshwater inputs from 16 rivers, including the Columbia, Fraser, and Puget Sound rivers, are forced with daily discharge and temperature time series from United States Geological Survey (USGS) and Environment Canada gauging stations. The Columbia and Fraser Rivers are the largest sources of freshwater to the coast. Dissolved nutrients (N) for the Fraser and Columbia Rivers are prescribed using a seasonal climatology of nitrate and nitrite derived from historical USGS and Environment Canada data. Using this climatology, the annual minimum/maximum for the Columbia River is 7/43 μM N and for the Fraser River is 8/32 μM N. Dissolved nutrients for all other rivers are set at a constant 5 μM N [*Sutton et al*., 2013].

One known deficiency in the 1.5 km Cascadia model is insufficient mixing within the Salish Sea and Strait of Juan de Fuca where the model grid resolution cannot resolve steep bathymetry [*Giddings et al*., 2014]. The lack of mixing in the model is apparent in the near-surface (top 20 m) waters exiting the Strait that are warmer than observed; despite this deficiency, modeled exchange flow and stratification within the Strait and Eddy are consistent with observations below 20 m depth [see *Giddings et al*., 2014, Figure 6]. However, one consequence of the insufficient model mixing in the Strait is apparent in the biological fields. *Masson and Peña* [2009] use data collected during seven years of seasonal surveys to show that phytoplankton growth seaward of the Victoria Sill at the eastern end of the Strait is significantly reduced—possibly due to light limitation from elevated levels of mixing and a relatively deep surface mixed layer. This "blue zone" of low growth was not captured in the Cascadia model due to insufficient mixing in the Strait and thus, a "no-growth" boundary condition was added to the Strait (east of −123.5°E) to enforce this important observed feature. Victoria Sill is thus the effective eastern boundary for biological fields in the model.

2.4. Overview of Numerical Experiments

Hindcasts of years 2004–2007 were performed. The first year of simulation (2004) is used as a biological spin-up, so the following discussion will focus on the last 3 years (2005–2007). Years 2005–2007 each represent very different climatological forcing conditions. In 2005, the onset of the "spring transition," typically signified by lowered sea level and the spin-up of a vertically sheared equatorward coastal jet, occurred approximately 50 days later than the climatological average off Newport, Oregon [*Kosro et al*., 2006]. There was an even further delay (another 50 days) before the dense, nutrient-rich upwelled water penetrated the surface, having significant impact on biological systems including phytoplankton productivity [*Thomas and Brickley*, 2006], zooplankton anomalies [*Mackas et al*., 2006], and the reproductive success of marine birds [*Sydeman et al*., 2006]. 2006 represents a year with strong spring and summer upwelling conditions and relatively low Fraser River discharge, while record snowpack in winter 2007 led to very high river flows in spring and summer 2007, but with more moderate upwelling conditions.

To examine freshwater influence in the Pacific Northwest coastal waters, we also performed two special cases of the simulation for each year in which we turned off the Columbia River transport (a coastal wall was created at the Columbia River mouth, as in *Banas et al*. [2009a, 2009b]), referred to below as the "No Columbia Case," and another in which we placed a coastal wall at the mouth of the Strait of Juan de Fuca to eliminate the influence of the Fraser and Puget Sound Rivers as well as any flow through the Strait, referred to as the "No Salish Case." It is important to note that in the No Salish Case, without estuarine circulation in the Strait, the Juan de Fuca Eddy does not form, as previously found by *Foreman et al*. [2008]. The full simulation with all rivers included is called the "Base Case." Each case ran continuously from 2004 to 2007. Numerical passive dye tracers were included in the "Base Case" simulations to separately track water

Table 3. Model-Observation Comparisons

	Willmott Skill Score		RMSE		
	All Data	Top 20 m	All Data	Top 20 m	Number of Samples
Water temperature	0.97	0.91	0.78°C	1.35°C	1305 CTD casts
Salinity	0.94	0.88	0.52	1.36	1305 CTD casts
Nitrate	0.93	0.83	5.17 μM N	4.29 μM N	944 bottle samples; 541 in top 20 m
Chlorophyll-*a*	0.73	0.58	2.69 μg L^{-1}	4.54 μg L^{-1}	1177 bottle samples; 779 in top 20 m

originating from the Columbia and Fraser Rivers, and a third dye tracer tracks water in all other Puget Sound Rivers combined.

2.5. Quantifying Growth, Grazing, and Primary Productivity

Primary productivity is estimated within the model from the phytoplankton growth rate and phytoplankton biomass, as $PProd = \mu_i P$, where P is converted to grams of carbon using a Redfield C:N ratio. Phytoplankton growth is limited by nitrogen availability in Pacific Northwest waters, and this nitrogen limitation can be quantified as,

$$L_N = 1 - \frac{N}{k_{s,app} + N} \tag{7}$$

where, $L_N = 0$ indicates no nitrogen limitation.

3. Model Validation

In this section, the strengths and weaknesses of the ecosystem model are evaluated using hydrographic data and biological observations from shipboard surveys and moorings associated with the Ecology and Oceanography of Harmful Algal Blooms-Pacific Northwest (ECOHAB-PNW) and River Influences on Shelf Ecosystems (RISE) projects (May–September 2004–2007). To assess model skill we use the Willmott Skill Score (*WSS*) [*Willmott*, 1982], defined as,

$$WSS = 1 - \frac{\frac{1}{N}\sum_{i=1}^{i=N}(m_i - o_i)^2}{\frac{1}{N}\sum_{i=1}^{i=N}(|m_i - \bar{o}| + |o_i - \bar{o}|)^2} = 1 - \frac{MSE}{\frac{1}{N}\sum_{i=1}^{i=N}(|m_i - \bar{o}| + |o_i - \bar{o}|)^2} \tag{8}$$

where o_i is an observation, m_i is the corresponding model value, there are N paired modeled/observed values, and *MSE* is the mean square error. The *WSS* is a measure of the level of agreement between the observed and modeled values, with a value of 1 indicating perfect agreement and a value of 0 indicating no agreement. There are many choices for model skill measures [*Stow et al*., 2009] but the *WSS* provides an intuitive index for comparison and incorporates the mean bias between modeled and observed values and the variability about that mean bias [*Willmott*, 1982]. In addition to *WSS*, in Table 3, estimates of root-mean-square error (RMSE) are reported for comparison between modeled and observed fields.

An extensive validation of the physical circulation model including comparisons to moored current meters, conductivity-temperature-depth sensors (CTDs), tide gauges, and satellite data is detailed in *Giddings et al*. [2014]. That study shows that the Cascadia model successfully captures both tidal and event-scale variability in sea surface height ($WSS = 0.97$) as well as the vertical structure of temperature, salinity, and currents ($WSS = 0.77$ and 0.58 for major and minor axis velocities, respectively) in the coastal Pacific Northwest. Additionally, the model reproduces key features of the PNW coastal ocean such as the seasonal upwelling of cold, nutrient-rich waters along the coast, freshwater features such as the Juan de Fuca eddy and Columbia River plume and the magnitude, location, and seasonal development of the California Undercurrent [*Giddings et al*., 2014]. A skill assessment of the oxygen segment of the ecosystem model is included in *Siedlecki et al*. [2014]. Here we will compare hindcast model results from 2005 and 2006 to observed temperature and salinities from CTD casts and to nutrient and chlorophyll *a* concentrations from water samples and moorings.

Comparisons of observed temperature, salinity, nitrate, and chlorophyll *a* from all CTD casts and water samples taken within the model domain (see locations in Figure 1) for years 2005–2006 are shown in Figure 3. Modeled values were extracted to match the collection time, location, and depth of the observations. The

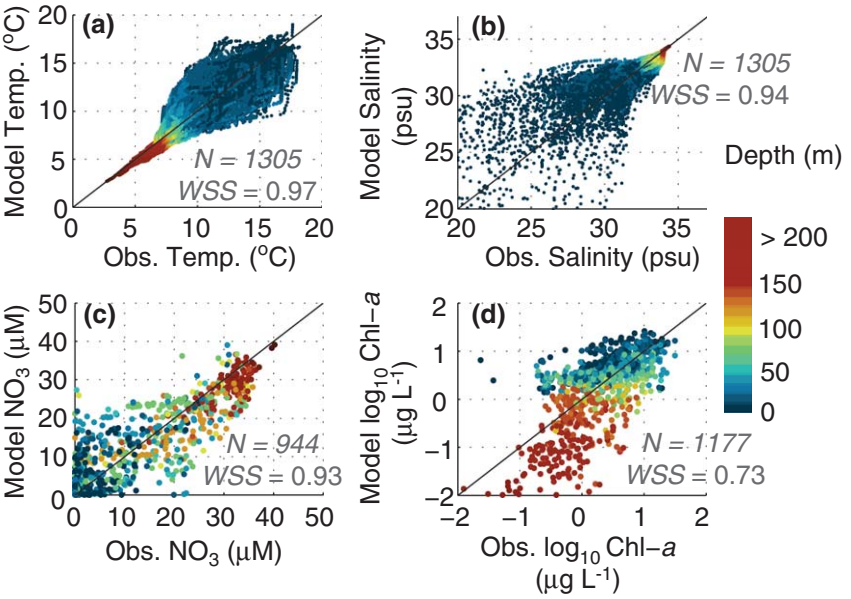

Figure 3. Observed versus modeled (a) water temperature, (b) salinity, (c) nitrate, and (d) chlorophyll *a* for all 2005 and 2006 CTD casts and bottle samples. Number of CTD casts for (a and b) or water samples for (c and d) are indicated by *N*, and Willmott Skill Score by *WSS*.

WSS and number, *N*, of CTD casts (which include multiple samples in the vertical for temperature and salinity, Figures 3a and 3b) or water samples (for nitrate and chlorophyll *a*, Figures 3c and 3d) for each parameter are shown in Figure 3 and also detailed in Table 3. One limitation of the Willmott score when applied to bulk ocean parameters, is that it aggregates important features of the vertical stratification and can reflect the general reproduction of the parameter with depth. To account for this effect and to assess model performance in the near-surface region, Table 3 reports *WSS* and *RMSE* values separately for the top 20 m in as well as for the entire water column. Additionally, cross-shelf sections of modeled and observed parameters are shown in Figure 4 for a cross-shelf ship track along 47°N on 6 August 2005, during a period of upwelling-favorable wind forcing.

3.1. Coastal Temperature and Salinity Structure

Figures 3a, 3b, and 4a demonstrate that modeled temperature and salinity fields are biased slightly cold and fresh, respectively (see also *Giddings et al*., 2014, Figure 5], but overall the model exhibits high skill ($WSS \geq 0.94$) in predicting the observed temperature and salinity fields, indicating that it is adequately capturing important features of coastal stratification and successfully reproducing the seasonal upwelling of dense water onto the shelf (Figure 4a). *WSS* for the top 20 m alone are slightly reduced, 0.91, but indicate that the model is adequately predicting surface water properties.

3.2. Nitrogen

A comparison of nitrate concentrations from 944 bottle samples to matching model estimates in Figure 3c shows that modeled nitrate is biased approximately 5 μM low at depth and biased high for observed nitrate values lower than 10 μM, typically near the surface. The spread in the modeled versus observed nitrate values in Figure 3c increases at shallower depths (the same is true for temperature and salinity in Figures 3a and 3b), highlighting the challenge of reproducing the exact spatial and temporal variability of dynamic near-surface features such as river plumes and fronts. Generally, however, model agreement with observed nitrate values is high ($WSS = 0.93$) and a snapshot of the nitrate field during an upwelling event in August 2005 (Figure 4b) suggests that the model shows appropriate nutrient stratification across the shelf.

In 2006, five oceanographic cruises performed water sampling for nitrate within the Strait of Juan de Fuca—ECOHAB-PNW in September 2006 and the Canadian Institution of Ocean Sciences (IOS) in April, June, September, and November 2006. We use this data to test the model skill at reproducing the observed nitrogen distribution in the Strait as it is of particular importance to the discussion below. Model-

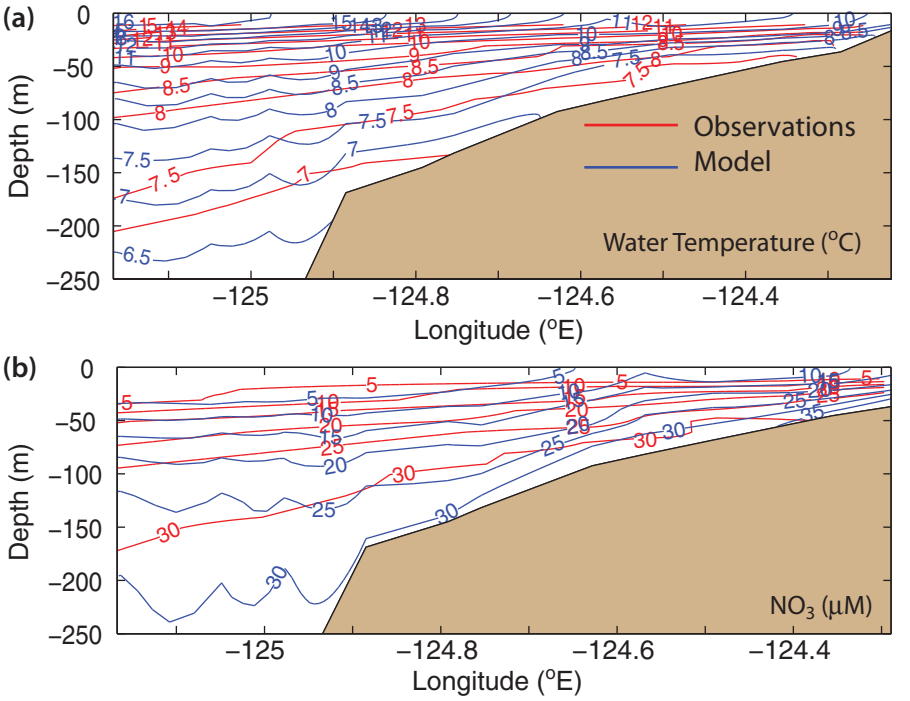

Figure 4. Cross-shelf sections at Line 47°N (green line in Figure 1). Modeled (blue) and observed (red) (a) water temperature and (b) nitrate concentration for 6 August 2005. In this figure, modeled fields are not subsampled to observations.

observational comparisons of nitrate concentrations from an IOS cruise on 13–14 June 2006 in a section down the center of the Strait are shown in Figures 5a and 5b (section line shown in Figure 1). While the observations exhibit more spatial variability than the modeled nitrate field, the model reproduces the vertical distribution of nitrate within the Strait, especially near the mouth. Point-by-point comparisons of nitrate

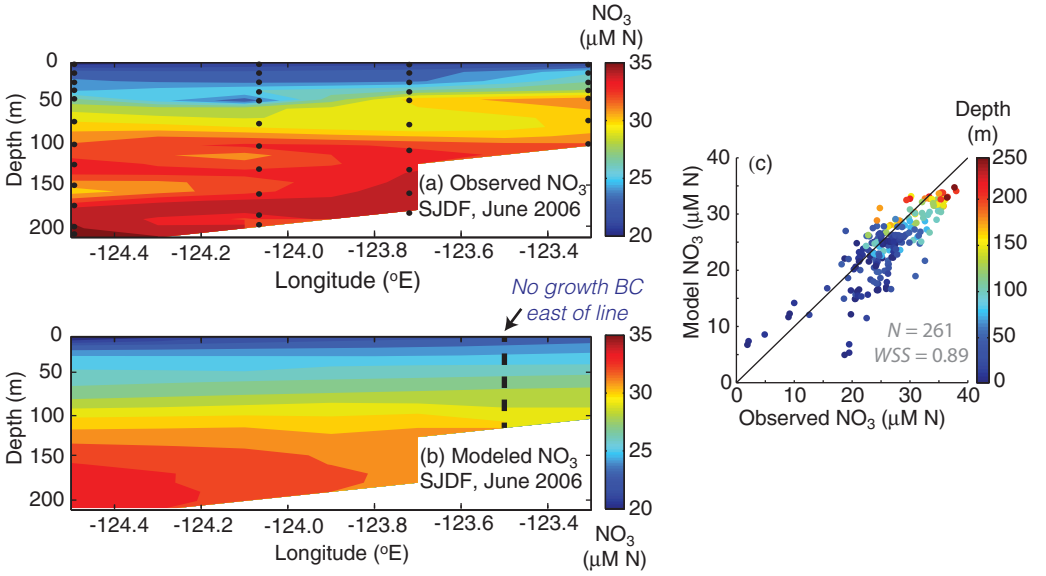

Figure 5. Nitrate concentrations in the Strait of Juan de Fuca. (a) Observations of nitrate from bottle samples taken along the centerline of the Strait (see green line in Figure 1) during a 13–14 June 2006 cruise from the Institute of Ocean Sciences (Fisheries and Oceans Canada, Sidney, BC) and (b) modeled nitrate concentrations from the same locations and times. Black dots in Figure 5a show the locations of bottle samples and where model results were extracted. Black dashed line in Figure 5b indicates where the "no growth" boundary condition discussed in section 2 is applied. (c) Modeled versus observed nitrate concentrations for 261 nitrate bottle samples collected within the Strait during an ECOHAB-PNW cruise (September 2006) and four IOS cruises (April, June, September, and November 2006).

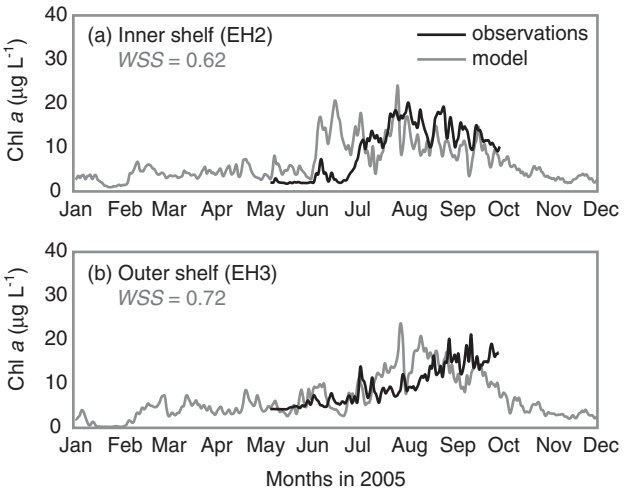

Figure 6. Time series of observed and modeled chlorophyll *a* at 4 m depth at (a) mooring EH2 and (b) EH3 on the Washington shelf (locations in Figure 1). Modeled chlorophyll *a* was extracted at the nearest horizontal and vertical grid point to the moorings.

values from all 2006 cruises and all seasons (Figures 5c) illustrate that the modeled nitrate in the Strait is biased approximately 5 μM low, consistent with the model performance at depth offshore.

3.3. Biological Stocks and Rates

Model chlorophyll *a* is estimated from phytoplankton biomass (as nitrogen) using a chlorophyll-to-nitrogen ratio, chl:N = 2.5 mg chl (mmol N)$^{-1}$, derived from measurements of particulate organic carbon (POC), particulate organic nitrogen (PON), and chlorophyll collected during the RISE experiment [*Banas et al.*, 2009b]. A point-by-point comparison of model chlorophyll *a* concentrations to 1177 bottle samples in Figure 3d shows reasonable agreement (*WSS* = 0.73; *RMSE* = 2.69 μg L^{-1}), but also reveals a depth-dependent bias in the model. Chlorophyll *a* values in surface waters (blue, green, and yellow dots) are biased high (*RMSE* = 4.54 μg L^{-1} in top 20 m), while model estimates of chlorophyll *a* at depth (orange and red points) are persistently biased low, indicating that the model tends to produce phytoplankton blooms shallower than in observations. The tendency of the model to under-predict the depth of phytoplankton blooms could reflect the corresponding model bias for low nitrate at depth or it could be related to the simplicity of the light attenuation parameterization within the model.

Time series of modeled chlorophyll *a* were compared to calibrated fluorescence observations at two locations on the Washington shelf, Mooring EH2 on the inner shelf and Mooring EH3 on the outer shelf near the Juan de Fuca Eddy (Figure 6; mooring locations in Figure 1). The model generally predicts the observed magnitudes and timing of bloom events, and seasonal trends in chlorophyll *a* at both locations (*WSS* = 0.62 and 0.72, respectively); however, it overpredicts the magnitude of phytoplankton biomass at both locations on the shelf during the delayed upwelling conditions of early summer 2005. The timing of model blooms and the magnitude of biological stocks (*P* and *Z*) are dependent upon modeled growth (μ) and grazing (g) rates, along with sinking, remineralization, and physical retention. Model growth rates are generally in the same range as those measured during deckboard dilution experiments carried out during ECOHAB-PNW and RISE cruises and reproduce the trend of increasing growth rate with increased nitrogen availability [*Banas et al.*, 2009a]. The mean model grazing rate is within one standard deviation of the expected value from dilution experiments, but shows lower variability than in observations.

Lastly, we compare modeled primary productivity, calculated from phytoplankton biomass and growth rates, to shipboard estimates of surface primary productivity from ^{14}C uptake experiments, made along Line 47N during three separate passes on a RISE cruise in August 2005 (Figure 7) [*Kudela et al.*, 2006]. Modeled surface primary productivity values, averaged over the month of August 2005, fall within one standard deviation of the bin-averaged values, indicating that the model largely captures the cross-shelf gradient in primary productivity during an upwelling period.

4. Results

4.1. Freshwater Presence in the Coastal Ocean

In the Pacific Northwest, the coastal waters are strongly influenced by freshwater inputs from the Strait of Juan de Fuca (fed by the Fraser River and other Salish Sea rivers) and the Columbia River. Figure 8 shows the percentage of time that surface salinity is less than 31.5, averaged by season over the 2004–2007 Base Case (realistic hindcast) simulations. Freshwater influence is high along the Washington and Vancouver Island coasts during the fall and winter, when downwelling-favorable wind events force buoyant freshwater

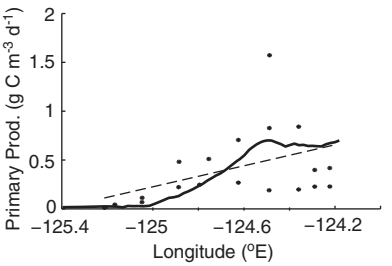

Figure 7. Modeled primary productivity (bold black line) is averaged over the month of August 2005. Primary productivity measurements by *Kudela et al*. [2006] collected throughout August 2005 (points) in a transect along Line 47°N (green line in Figure 1). Linear least-squares fit of *Kudela et al*. [2006] observations plotted for reference (dashed line).

plumes to the north and onshore, whereas in the summer, upwelling-favorable wind events push freshwater plumes to the south and offshore resulting in more diffuse freshwater presence along the coasts and greater freshwater influence offshore [*Banas et al*., 2009b; *Hickey et al*., 2005; *Hickey*, 1989]. Winds are more variable in spring and, thus, freshwater influence extends to the north and south of the source regions. The Vancouver Island Coastal Current (VICC), a poleward-flowing, buoyant plume that hugs the western coast of Vancouver Island, develops seasonally in response to buoyancy flux from the relatively fresher outflow from the Strait of Juan de Fuca [*Hickey et al*., 1991]. The results in Figure 8 are not highly sensitive to the cutoff salinity value (31.5) and are consistent with passive dye tracers released in the rivers. It is important to note that the model does not include Oregon rivers and thus probably underestimates the influence of freshwater south of the Columbia River mouth [*Wetz et al*., 2006].

4.2. Coastal Productivity

To examine the role of freshwater input on regional patterns of biological productivity, we used the Cascadia ecosystem model to compare fields of primary productivity and nitrogen limitation (see section 2.5 for definitions) between three numerical cases: Base Case, No Columbia Case, and No Salish Case. Figures 9a–9c show vertically integrated maps of primary productivity averaged over the 2005 growing season (April–September) for each simulation case. In the realistic hindcast Base Case (Figure 9a), primary productivity is highest in a band adjacent to the coast and in the Juan de Fuca Eddy region, at approximately 3–5 g C m^{-2} d^{-1}. Note that because a "no growth" biological boundary condition was imposed east of 123.5°W (see section 2.3 for details), primary productivity or nutrient limitation results are not shown for this area (Figures 9 and 10).

4.2.1. The Columbia River

The magnitude and spatial patterns of primary productivity in the No Columbia Case (Figure 9b) are quite similar to the Base Case (Figure 9a), on the scale of the model domain. The most substantial differences in primary productivity between the two runs appear in the area immediately surrounding the mouth of the

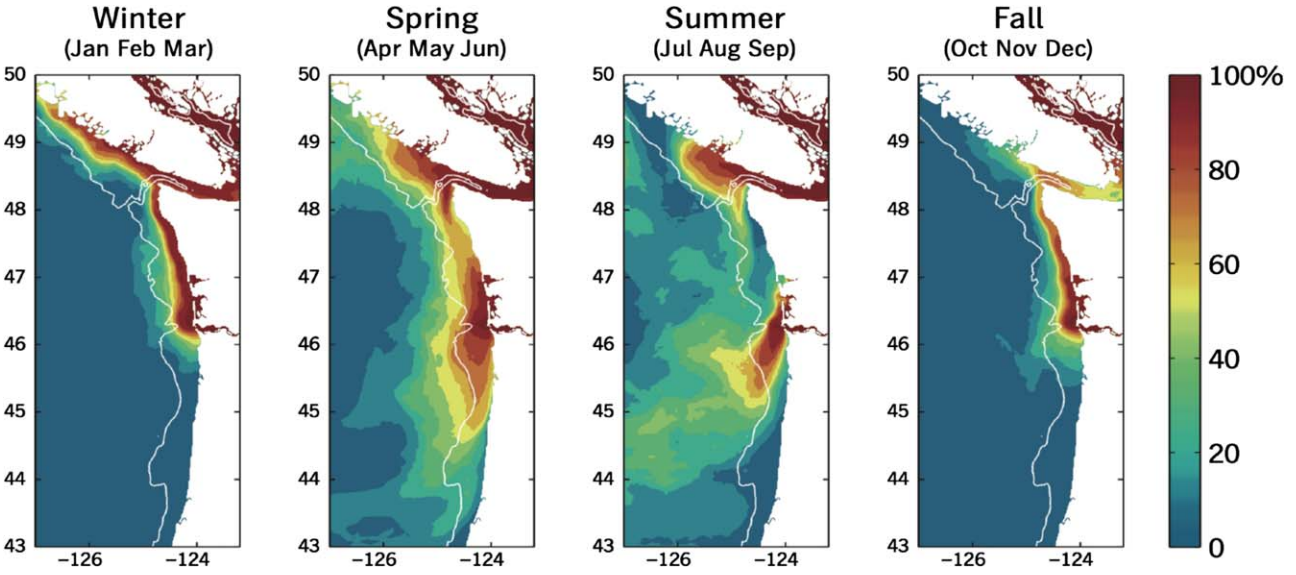

Figure 8. 2004–2007 seasonally averaged "River Index" (% of time with surface salinity < 31.5).

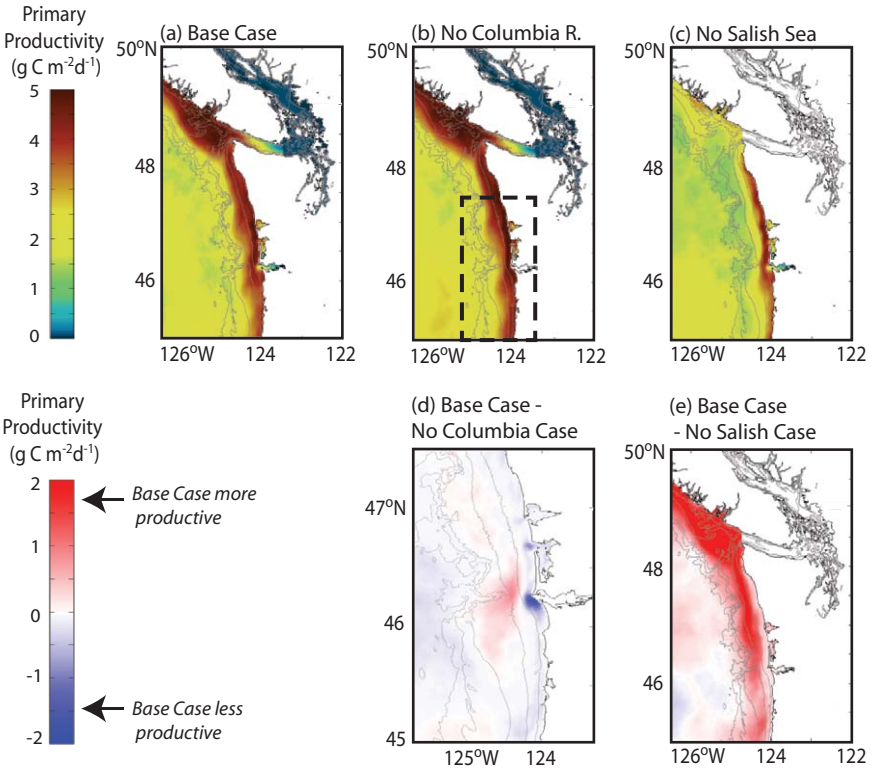

Figure 9. Depth-integrated primary productivity, for three model cases: (a) Base Case, (b) No Columbia Case, and (c) No Salish Case. Bottom plots represent the difference in primary productivity (d) between the Base Case and the No Columbia Case (expanded view of area near Columbia River mouth, indicated by dashed box in Figure 9b) and (e) between the Base Case and the No Salish Case. Depth contours are at 50, 100, 200, 500, and 1000 m.

Columbia (Figure 9d): on the inner shelf, within 10 km of the mouth of the Columbia River, primary productivity is approximately 2 g C m^2 d^{-1} higher in the No Columbia Case than in the Base Case (blue patch), and on the middle to outer shelf, productivity is reduced in the No Columbia Case by approximately 0.7 g C m^{-2} d^{-1} compared to the Base Case (pink patch). These patterns suggest that the Columbia River plume effectively displaces production farther offshore in a patchy band from 45°N to 47°N, supporting findings by *Banas et al*. [2009a], who made a similar comparison for a month of summer conditions in 2004.

Maps of nitrogen limitation at the surface indicate that phytoplankton growth in the near-field Columbia plume is more nutrient-limited in the No Columbia Case than in the Base Case (Figure 10d), consistent with observations by *Lohan and Bruland* [2006] who attributed elevated nitrate levels (as high as 20 μM) in the near-field plume to mixing processes at the tidal plume edge [*MacCready et al*., 2009; *Orton and Jay*, 2005]. Farther offshore, nitrogen limitation is slightly decreased by inclusion of the Columbia River, consistent with the offshore displacement of primary production.

4.2.2. Strait of Juan de Fuca

Average primary productivity in the No Salish Case (Figure 9c) is drastically reduced from the Base Case (Figure 9a) in the Juan de Fuca Strait and Eddy region, by as much as 3 g C m^{-2} d^{-1}, and along the middle to outer Washington and Oregon shelves (seaward of the 50 m isobath), by 1–2 g C m^{-2} d^{-1} (difference between runs shown in Figure 9e). Primary productivity averaged over the whole model domain, excluding the Salish Sea and grid cells very near boundaries, is 20% lower in the No Salish scenario compared to the Base Case, a consequence of reduction in both phytoplankton biomass and phytoplankton growth rate. Time series of volume-averaged primary productivity in 2005 in four areas of interest: the Vancouver Island shelf, the Juan de Fuca Eddy, the Washington shelf, and the Oregon shelf (Figure 11), highlight substantial regional differences in the influence of the Strait outflow. Large differences between Base Case and No Salish Case productivity in the eddy region (Figure 11b) are not surprising given that there is no eddy in the latter case; however, more interesting, is the apparent influence of Strait outflow over the shelf regions.

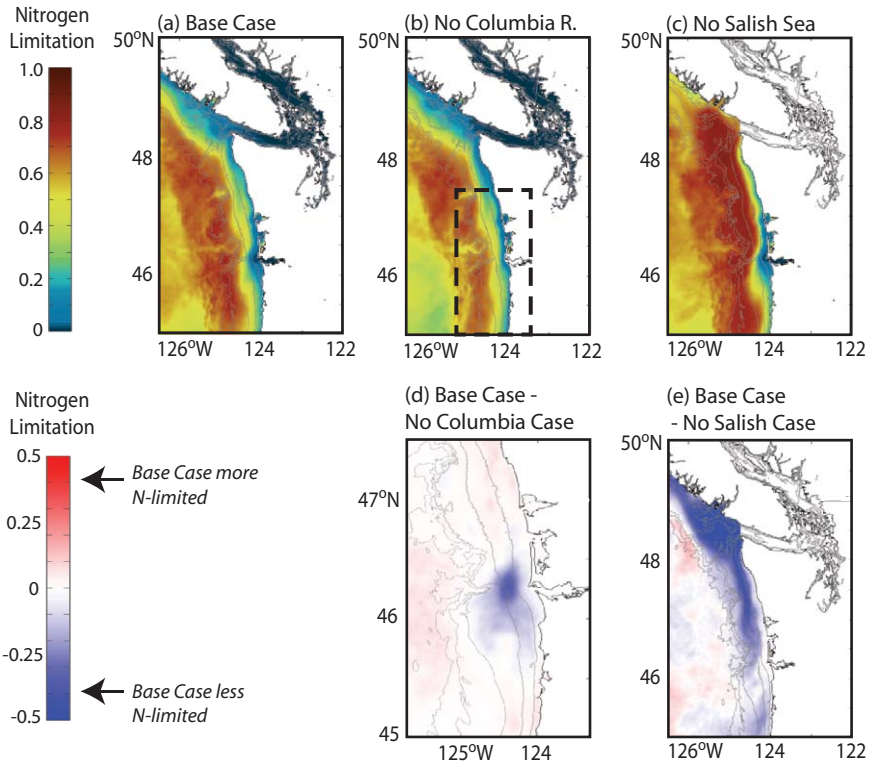

Figure 10. Nitrogen limitation in the near-surface waters (upper 10 m), for three model cases: (a) Base Case, (b) No Columbia Case, and (c) No Salish Case. Bottom plots represent the difference in nitrogen limitation (d) between the Base Case and the No Columbia Case (expanded view of area near Columbia River mouth, indicated by dashed box in Figure 10b) and (e) between the Base Case and the No Salish Case. Depth contours are at 50, 100, 200, 500, and 1000 m.

Volume-averaged primary productivity is reduced in the absence of the Strait outflow by 44% on the Vancouver Island shelf (Figure 11a), by 32% on the Washington shelf (Figure 11c), and by 18% on the Oregon shelf (Figure 11d) over the 2005 growing season. These results reinforce the idea that Salish Sea outflow affects coastal productivity in the near-field; but also suggests that it can modify coastal productivity over 400 km to the south.

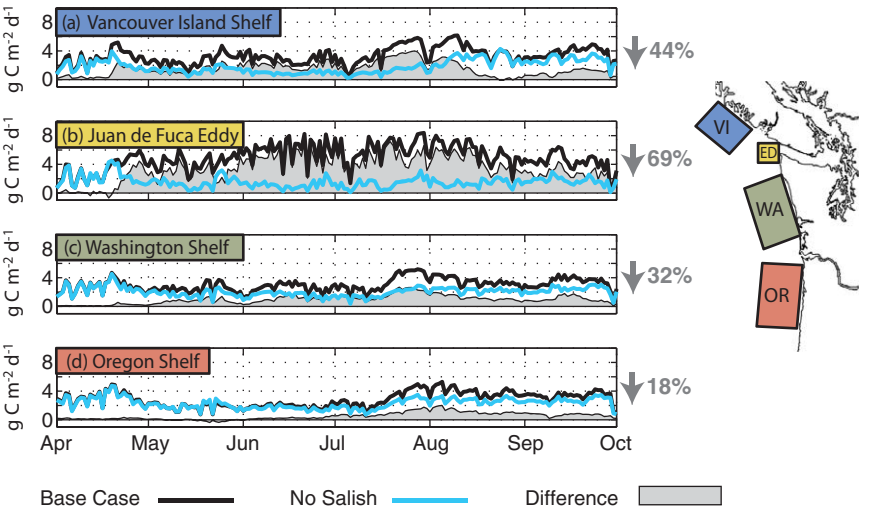

Figure 11. Time series of volume-averaged primary productivity for Base Case and No Salish Case in different regions of the Pacific Northwest coast for 2005. Percentages to the right-hand side of the time series indicate the total reduction in primary productivity in the No Salish Case compared to the Base Case for each region.

Maps of surface nitrogen limitation for the No Salish Case (Figure 10c) show increased nitrogen limitation in the Juan de Fuca Strait and Eddy region as well as along the middle to outer Washington and Oregon shelves when compared to the Base Case (Figure 10a; difference between these runs shown in Figure 10e), implying that one important aspect of the Salish Sea outflow to coastal biological productivity is its contribution to nutrients in the euphotic zone.

5. Discussion

The major sources of riverine water to the coastal Pacific Northwest are the Columbia River and the rivers of the Salish Sea, which can be seen through all seasons as low surface-salinity features (Figure 8). The role that each of these rivers play in shaping biological productivity on the PNW shelf is very different as evidenced by results from three numerical experiments presented above (Figures 9 and 10). In the discussion that follows we will look more closely into the processes through which these rivers influence coastal productivity in PNW coastal waters.

5.1. The Columbia River Plume Redistributes Regional Productivity

The Columbia River is important region-wide as a source of micronutrients, primarily iron and silica, to the coastal ocean [*Bruland et al*., 2008; *Chase et al*., 2007]. Additionally, the Columbia plume affects the distribution of phytoplankton biomass to the north and south of the river mouth by acting as a low-density front which modifies the alongshore current and wind-driven surface currents [*Hickey et al*., 2005; *Small and Menzies*, 1981] and by retaining blooms within the river plume itself [*Kudela et al*., 2010]. Regional-scale effects on the spatial distribution of primary production are evident in results from our numerical experiments (Figure 9), as in a previous version of the model [*Banas et al*., 2009a, 2009b], which show that the Columbia plume effectively shifts biological productivity farther offshore. These runs also suggest, that during the upwelling season (April–September), the Columbia plume does not affect nitrogen-limited biological productivity along the PNW coast as strongly as does outflow from the Salish Sea. However, it is important to note that since this model does not resolve iron or silica dynamics, the influence of these micronutrients on regional productivity was not tested here.

The Columbia River may play an important role in coastal productivity in the winter and spring. *Anderson* [1964] shows some evidence that effluent from the CR in winter and spring can enhance phytoplankton biomass and productivity on the inner shelf of WA, but he attributes this productivity to a shallower mixed layer and greater temperatures within the plume. That study also concluded that the major effect of the Columbia River effluent is on the timing of phytoplankton blooms rather than any gross differences in annual production between oceanic waters and plume waters.

5.2. Nitrogen Flux in the Juan de Fuca Strait and Eddy Region

Evidence from numerical experiments presented in section 4 shows outflow from the Strait of Juan de Fuca to be an important source of nitrogen to the coastal euphotic zone, accounting for almost half of primary productivity on the Vancouver Island shelf, a third of productivity on the Washington shelf, and a fifth of productivity on the Oregon shelf.

To characterize the sources and fate of water flowing out of the Strait and examine its importance as a source of nutrients for the coastal waters of the Pacific Northwest, a budget for total nitrogen ($TN = N + P + Z + SD + LD$) is constructed for an area in the Juan de Fuca Strait and Eddy region ("JDFSER," the dark gray box outlined in Figure 12a). The simplified *TN* budget can be expressed as:

$$\frac{\partial}{\partial t}\int_V TN\,dV \approx \oint \overrightarrow{u}\,TN \cdot \overrightarrow{dA} - \int_{A_{bed}} \left(F^{benthic}_{denitr} z_{(k=1)}\right) dA_{bed} \tag{9}$$

where the left-hand side of equation (9) represents the time rate of change of *TN* storage within the volume defined by the JDFSER box from sea surface to bottom and the first term on the right-hand side represents the advective flux of *TN* through a closed path defined by the box in Figure 12a. Note that in the discussion below, we also refer to advective fluxes through separate sections or "faces" of this box, defined in Figure 12a as: Strait of Juan de Fuca face (JDF), the Vancouver Island Coastal Current face (VICC), the western face (WF), and the southern face (SF)). The last term on the right-hand side of equation (9) represents nitrogen

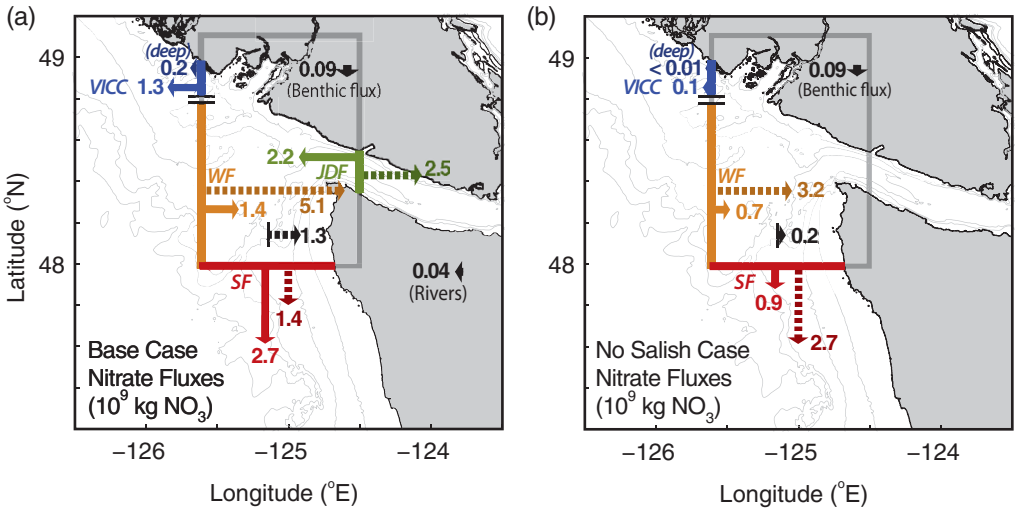

Figure 12. Nitrate fluxes (in 10^9 kg NO_3) in the near-surface zone ($\leq$50 m; solid arrows), deeper than 50 m (dashed arrows), benthic fluxes within the box (solid black arrow in box, this flux is oriented into the bed), in a section of the Juan de Fuca Canyon (black dashed arrow) and from all rivers (black arrow) for the (a) Base Case and the (b) No Salish Case. Colored labels denote names of flux faces: Strait of Juan de Fuca (JDF, green), Vancouver Island Coastal Current (VICC, blue), West Face (WF, orange), and South Face (SF, red). Fluxes are integrated over the upwelling season (April–September) and averaged over the years 2005–2007.

losses due to benthic fluxes (equation (5)). The storage term and advective fluxes of *TN* are calculated from vertically resolved, subtidal time series of simulated currents and all components of total nitrogen (computed with a Godin low pass filter; [*Emery and Thomson*, 2004]). The western-most face of the box has been divided into two sections in order to distinguish the flux through the fresher VICC. The division of WF and VICC sections (at 48.8°N along the western-most face) was informed by seasonally averaged salinity and current fields (e.g., Figure 8). Diffusive fluxes of total nitrogen were found to be three to four orders of magnitude smaller than advective fluxes and are therefore neglected in (equation (9)). Residuals in the *TN* budget, likely due to temporal filtering, are less than 5% of the rate of change of *TN* within the volume (term on left-hand side of equation (9)), while advective fluxes account for over 90% of *TN* variance within the JDFSER region.

Table 4 summarizes fluxes of *TN* into the JDFSER control volume for the 2005–2007 Base Case runs, and, for reference, also lists the advective fluxes of *TN* for a section of the Juan de Fuca Canyon (at the location of the black dashed arrow in Figure 12a, from the canyon rim to the bottom) and for rivers. The *TN* fluxes are integrated over the "growing" season (April–September) for each year of the simulation (2005–2007). The advective fluxes are separated by depth into fluxes in the "near-surface" zone ($\leq$50 m) and in the "deep" zone ($>$50 m). Fifty meters was chosen as the nominal division between surface and deep fluxes as this is the approximate depth of the zero-crossing for the exchange flow currents near the mouth of the Strait of Juan de Fuca. The true euphotic zone, defined by the depth at which light intensity falls to 1% of surface levels, varies from 10 to 100 m in CTD PAR data in the JDFSER, but is on average 30 m deep and is largely contained within the "near-surface" zone.

5.3. Salish Sea Estuary as a Source of Upwelled Nitrogen

Figure 12 illustrates the fluxes of nitrogen in the JDFSER control volume for the 2005–2007 Base Cases (Figure 12a) and No Salish Cases (Figure 12b). The fluxes are calculated here in kg of NO_3 for comparison to previous estimates and observations in the literature and later in this manuscript fluxes are reported in kg of *TN* for inclusion of all forms of nitrogen. The conversion between fluxes of *TN* (Table 4) and fluxes of NO_3 (Figure 12) is: 1 kg *TN* = 4.3 kg NO_3. *N* fluxes in Figure 12 are integrated over the "growing season" (April–September) and then averaged over all 3 years.

Realistic hindcasts of circulation (Figure 12a) show that, on average over the 2005–2007 growing season (April–September), nitrate is fluxed into the JDFSER volume through the near-surface zone of the Strait (JDF) and through the west face (WF) due to the southeastward flow of the California Current and by wind-driven upwelling at depth. Nitrate flux out of the JDFSER occurs primarily through the south face (SF) and

Table 4. Fluxes of Total Nitrogen (10^8 kg N), April–September, Base Case[a]

Section	Depth Zone	2005	2006	2007	Average
Juan de Fuca Strait (JDF)	Near surface	4.5	5.3	5.6	5.1
	Deep	−5.0	−5.9	−6.3	−5.7
Vancouver Is. Coastal Current (VICC)	Near surface	−3.0	−3.5	−3.1	−3.2
	Deep	−0.5	−0.5	−0.5	−0.5
West Face (WF)	Near surface	2.3	3.8	6.1	4.1
	Deep	6.9	12.6	15.4	11.6
South Face (SF)	Near surface	−5.2	−7.3	−10.6	−7.7
	Deep	1.1	−5.3	−5.8	−3.3
Benthic Flux	At Bed	−0.9	−0.9	−0.9	−0.9
Other fluxes for comparison					
Juan de Fuca Canyon	Below canyon rim	2.9	3.1	2.9	3.0
Fraser + Salish Sea Rivers		0.1	0.1	0.1	0.1
Columbia River		0.2	0.2	0.2	0.2

[a]Note: fluxes are positive oriented into the control volume; canyon fluxes are positive directed to the east.

through the Vancouver Island Coastal Current (VICC), over 70% of which occurs in the near-surface zone. The nitrogen budget (equation (9)) implies a vertical flux of nitrogen within the JDFSER volume from the deep layer to the near-surface layer of approximately 5×10^8 kg NO_3 when integrated from April to September and averaged over all Base Case years.

The average flux of nitrate out of the Strait in the near-surface zone, 2.2×10^9 kg NO_3, predicted by the Cascadia model is on the same order as, but higher than, the conservative estimate made by *Mackas et al*. [1980], 0.5×10^9 kg NO_3. *Mackas et al*. [1980] assume a near-surface velocity in the Strait of 0.1 m s^{-1}, consistent with our model output, and a "minimal representative value" for surface nitrate concentration of 0.28 g m^{-3}, which is approximately a third of the average near-surface nitrate value in our model results and recent observations [*Masson*, 2006]. The direction of this difference is consistent with the no-growth condition imposed landward of Victoria Sill: our model most likely omits some amount of trapping of incoming nutrients within the Salish Sea estuary that would otherwise happen due to sinking and burial of detritus.

In simulation cases without a functioning Strait (No Salish Case, Figure 12b), where wind-driven coastal upwelling is the primary mechanism for supplying nutrients to the near-surface zone, the flux of nitrate through the Vancouver Island Coastal Current (VICC) and south to the coast of Washington (SF) in the upper 50 m of the water column is a quarter (25%) of that in the Base Case (Figures 12a and 12b). This suggests that near-surface export of nitrogen from the JDFSER volume to the surrounding shelves is approximately 4 times larger with estuarine circulation within the Strait than with wind-driven upwelling alone. Some of this difference may also be attributed to the vertical transport of nutrients within the JDF eddy (doming of the nutricline), which does not form in the No Salish Cases.

Temporal variability in wind forcing and freshwater discharge (Figures 13a and 13b) can alter regional circulation and modify nitrogen flux in the JDFSER. *Monteiro and Largier* [1999] and *Hickey et al*. [2002] noted in shallower estuaries attached to upwelling zones that upwelling/downwelling-driven variation in water properties at the estuary mouth can influence the baroclinic coupling between the coastal ocean and estuary and, thus, affect estuarine circulation. Nutrient cycling in rías in northwest Spain have been tied to the coupled dynamics of wind-driven upwelling and estuarine circulation [*Alvarez-Salgado et al*., 1996]. More locally, *Cannon* [1972] and *Alford and MacCready* [2014] observed that the deep flow in Juan de Fuca canyon, the deepest nutrient input into the Salish Sea estuarine circulation, responded strongly to upwelling/downwelling-favorable winds: upwelling-favorable winds drive up-canyon flow, consistent with the pattern of nitrate fluxes seen in the model. The fluxes of nitrogen in the deep and shallow layers of the Strait (Figure 13c) are significantly correlated with the alongshore wind index ($R^2 = 0.48$, significant at the 95% confidence level), where strong upwelling events are associated with the landward flux of nitrogen in the deep part of the Strait and the seaward flux of nitrogen in the near-surface zone [see also *Thomson et al*., 2007].

Submarine canyons along the PNW coast act to further enhance the upwelling of dense, nutrient-rich water onto the continental shelf (see observations in *Hickey* [1989], *Hickey and Banas* [2008], and modeling studies

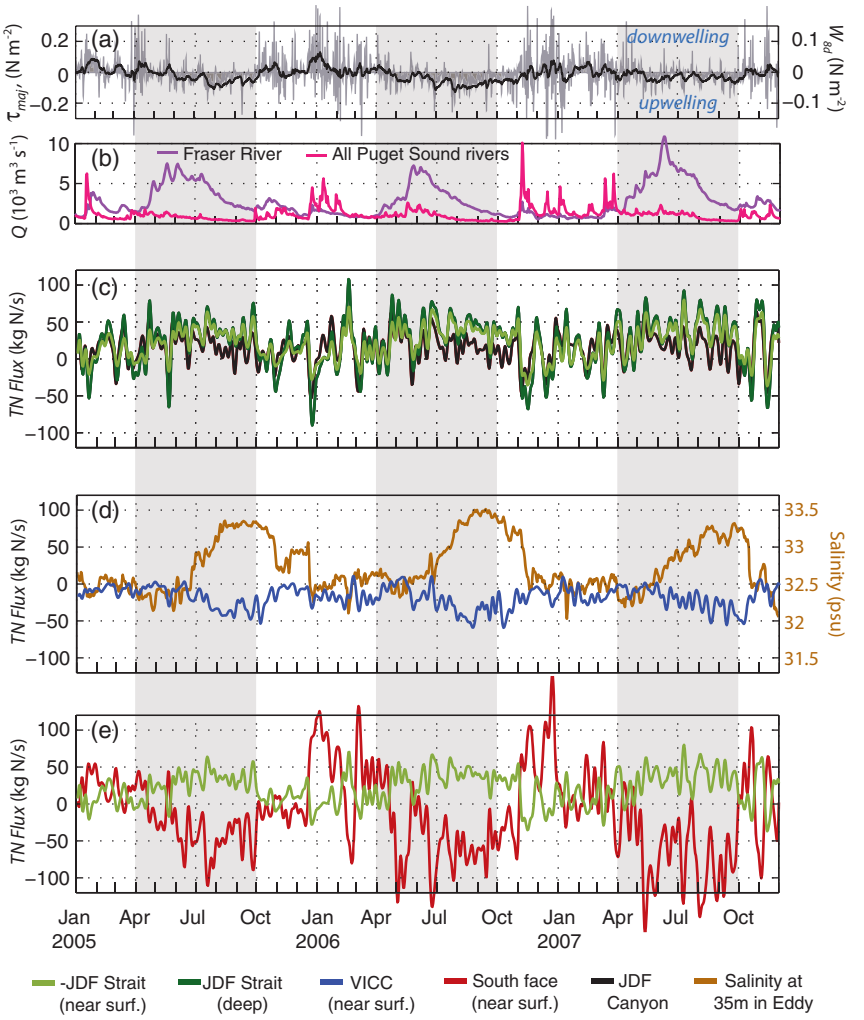

Figure 13. 2005–2007 time series of (a) alongshore wind stress (thin gray line) and 8 day cumulative wind index, W_{8d} (bold black line; based off of *Austin and Barth* [2002], but retaining units of stress, τ), (b) observed Fraser River and Puget Sound River discharges, (c-e) flux of total nitrogen (*TN*) through sections defined in Figure 12 and in the legend. Colors of *TN* flux time series correspond to flux face colors in Figure 12. All fluxes are 8 day low-pass filtered and positive to the north or east depending upon the orientation of the face except for the JDF Strait (near surface) which is plotted as the negative flux for ease of comparison to the JDF Strait (deep). Figure 13d also shows salinity at 35 m depth in the center of the Juan de Fuca eddy (brown line).

by *Allen* [1996] and *Connolly and Hickey* [2014]). In our simulations, the average flux of nitrate within the Juan de Fuca Canyon (black dashed arrow shown in Figure 12a and black line in Figure 13c) is directed onshore and into the Strait during the growing season and accounts for over 50% of the nitrate fluxed into the Strait at depth. Nitrate flux through canyon sections closer to the head (approaching the mouth of the Strait), capture an even larger fraction of nitrate flux into the Strait (not shown). This is in agreement with recent observations near the head of the Juan de Fuca Canyon by *Alford and MacCready* [2014], which demonstrate strong up-canyon transport and find the canyon to be a conduit for water from below 300 m depth to enter the Strait.

While the strong influence of the JDF Canyon on source waters into the Strait is not surprising given recent observations, what is interesting is that mass flux within the canyon seems to be affected by estuarine circulation within the Strait. In simulations without a functioning estuarine circulation (No Salish Cases), mass flux of nitrogen through a section of the Juan de Fuca Canyon over 40 km from the mouth of the Strait (Figure 12b, 0.2×10^9 kg NO_3,) is drastically reduced (15%) compared with canyon fluxes in the Base Case (Figure 12a). The difference in canyon fluxes between the two cases could be a due to a combination of many differences between the runs (estuarine exchange, existence of an eddy, changes in shelf stratification, alongshore currents, etc.), and calls for a careful mechanistic study that is outside of the scope of this paper.

5.4. Ocean Versus Land-Derived Nitrogen in the Strait of Juan de Fuca

The seasonally averaged fluxes in Figure 12 provide evidence of the dominant role of ocean-derived nitrogen in outflow from the Strait of Juan de Fuca. The annual-average nitrate from the 15 modeled rivers flowing into the Salish Sea, 4×10^7 kg NO_3, represents less than 2% of near-surface nitrate flux out of the Strait during the growing season (April–September). Our analysis suggests that the nitrogen exiting the Strait is almost entirely of ocean-origin; upwelled into the Strait at depth, mixed into surface waters by an energetic tidal mixing environment, and then returned to the coastal ocean in surface waters where it is available to support new production. The advective flux of *TN* out of the JDF Strait in the near-surface zone is of a similar magnitude, although slightly less than, the advective flux of *TN* into the strait at depth in all modeled years (see Table 4 for *TN*; a similar pattern for nitrate is shown in Figure 13a). (Note that the *TN* flux in the upper 50 m leaving the JDFSER is $\geq$94% in the form of dissolved nutrients, not PON, through all faces.) This result is further supported by the visually apparent and statistically strong correlation ($R^2 = 0.91$, significant at the 95% confidence level) between time series of *TN* advective fluxes in the deep (dark green) and near-surface (lighter green) zones of the JDF Strait (Figure 13c) for all simulated years, including winter.

We might expect the influence of river-originated nutrients to be maximal in the winter and early spring, when downwelling-favorable winds depress the coastal nutricline. However, the strong correspondence of *TN* flux in the near-surface and deep zones of the Strait throughout the year (Figure 13c) suggests that direct *N* input from the Salish Sea rivers (i.e., terrigenously sourced) are never a first-order input to the nitrogen flowing out of the Strait. Thus, while the input of low salinity, buoyant water from the Fraser and other Salish Sea Rivers is an essential element of estuarine circulation within the Strait and in the formation of the Juan de Fuca Eddy [*Foreman et al*., 2008], land-derived nitrogen carried by these rivers accounts for a very small fraction of nitrogen exiting the Strait (Figure 12a and Table 4).

5.5. Flow Reversals and the Flux of Ocean-Derived Nitrogen into the Salish Sea

Periods of flow reversal within the Strait of Juan de Fuca, where the exchange flow is opposite that of typical estuarine circulation; i.e., landward near the surface and seaward at depth, have been observed in winter and in summer [*Frisch et al*., 1981; *Holbrook and Halpern*, 1982]. *Thomson et al*. [2007] find that these flow reversals occur at the transitions from upwelling to downwelling-favorable wind conditions and are also often associated with the intrusion of lower salinity water from the Washington coast into the Strait. Reverse estuarine circulation occurs approximately five times per year in our numerical hindcasts of 2005–2007, happening primarily in winter when storms bring strong downwelling-favorable winds and can last for several days. During these reversal periods, nitrogen-rich water that has been mixed into the surface waters within the Strait, is transported into the Straits of Georgia and Puget Sound in the near-surface zone (Figure 13c).

5.6. Fate of Nitrogen Leaving the JDFSER

Using a circulation model and field-based drifter tracks, [*MacFadyen et al*., 2008, 2005] demonstrate that freshwater leaving the Strait of Juan de Fuca can be transported to the northwest in the VICC. Alternately, it can be advected around the margin of the Juan de Fuca eddy and either become entrained in the eddy or, under upwelling-favorable wind events, flow to the southeast, merging with the Washington coast shelf break jet. Results from the 2005 to 2007 simulations presented here are consistent with findings by *MacFadyen et al*. [2005] (also seen in *Giddings et al*. [2014]). Below, we will discuss the northern and southern transport pathways for nitrogen-rich water leaving the SJDF.

An average of 1.5×10^9 kg NO_3 is transported to the Vancouver Island shelf through the VICC from April to September (Figure 12a), peaking in late summer/early fall (blue line in Figure 13d). This estimate is 30% larger than approximations of nitrogen flux due to upwelling and tidal mixing along a 100 km length of the Vancouver Island shelf made by *Crawford and Dewey* [1989] and is consistent with their conclusion that the Strait is the primary source of nutrients to the Vancouver Island shelf. *TN* flux through the VICC in the model is not controlled by local winds (R^2 with $W_{8d} = 0.12$, *not* significant at the 95% confidence level, where W_{8d} is an 8 day cumulative upwelling index [*Austin and Barth*, 2002]), but rather by the seasonal development of the JDF eddy, as represented by a time series of salinity at 35 m depth near the center of the eddy (48.4°N, −125.2°E) [*MacFadyen and Hickey*, 2010]. As the JDF eddy spins up and grows in size throughout the summer, the doming of higher salinity water within the cyclonic eddy is associated with an increase in the transport of nitrogen in the VICC (Figure 13d, $R^2 = 0.46$, significant at the 95% confidence level).

The largest export of nitrogen from the JDFSER occurs to the south, toward the Washington/Oregon shelves in the near-surface zone (upper 50 m). We estimate that an average of 4.1×10^9 kg NO_3 is transported south to the Washington shelf from the JDFSER during the upwelling season (Figure 12a), 67% of which is in the upper 50 m. The flux of *TN* through the South Face is more highly variable than through the VICC, is more responsive to local wind forcing ($R^2 = 0.50$, significant at the 95% confidence level), and is also related to the flux of nitrogen exiting the Strait in the near surface zone ($R^2 = 0.67$, significant at the 95% confidence level, Figure 13e).

The enhancement of equatorward nitrate flux from the West Face to the South Face (2.7×10^9 to $1.4 \times 10^9 = 1.3 \times 10^9$ kg NO_3) is of similar magnitude to the fraction of surface-layer NO_3 flux out of JDF not entering the VICC (2.2×10^9 to $1.3 \times 10^9 = 0.9 \times 10^9$ kg NO_3) (Figure 12a). This suggests that the nitrate supply to the Washington shelf from freshwater-driven processes in the Strait is comparable to nitrate upwelled to the Washington coast via other mechanisms (e.g., local winds and canyon enhancement, which *Hickey and Banas* [2008] estimated to contribute approximately 0.8×10^9 kg NO_3 over the same seasonal period).

6. Conclusions

In this study, we introduce the ecosystem-component of the Cascadia Model—a coupled physical-biological model of the Pacific Northwest coastal ocean. The ecosystem model tracks nitrogen in five phases: dissolved nitrogen, phytoplankton, zooplankton, and large and small detritus—and has been validated using CTD data, nutrient and standing stock estimates from water samples and a wealth of biological rate data from deckboard experiments collected during several observational efforts on the Vancouver Island-Washington-Oregon shelves. We demonstrate that the Cascadia ecosystem model adequately simulates nitrogen distribution and the magnitude and timing of phytoplankton blooms in the PNW coastal region.

Using three years of realistic hindcasts together with experimental simulations in which outflow from the Columbia River and the Salish Sea are restricted, we examine the influence of these freshwater sources and estuarine circulation within the Strait on the biological productivity of the PNW shelf. Results from these numerical experiments suggest that outflow from the Strait of Juan de Fuca represents a critical source of nitrogen to the coastal PNW; accounting for almost half of the primary productivity on the Vancouver Island shelf, a third of productivity on the Washington shelf, and a fifth of productivity on the Oregon shelf from April to September. In our simulations, outflow from the Columbia River displaces primary productivity toward deeper water but does not have a major effect on total regional productivity via macronutrient supply beyond the near-field plume, consistent with *Banas et al*. [2009a] and *Hickey and Banas* [2008]. Note, however, that the Columbia River is an important source of micronutrients (iron and silica) for the region, which are not considered in this model.

From a total nitrogen budget constructed in the Juan de Fuca Strait and Eddy Region (JDFSER), we found that nitrogen exiting the Strait in the upper 50 m is almost entirely (98%) of ocean-origin; upwelled into the Strait at depth, mixed into surface waters by the energetic tidal mixing within the Strait, and then returned to the coastal ocean in surface waters where it is available to support new production. From the standpoint of nitrogen availability in the coastal euphotic zone, the estuarine circulation induced by riverine inputs to the Salish Sea is orders of magnitude more important than the supply of terrigenous nitrogen by rivers in the PNW.

Our model results suggest that the nitrogen-rich surface waters exiting the Juan de Fuca Strait and Eddy Region follow two primary pathways: to the northwest in the Vancouver Island Coastal Current and to the south toward the Washington and Oregon shelves. Nitrogen delivery to the Vancouver Island shelf through the VICC is linked to the seasonal development and circulation of the Juan de Fuca eddy, while the flux of total nitrogen south toward the coast of Washington is more highly influenced by local wind forcing. Results from our regional nitrogen budget suggest that the estuarine circulation driven by freshwater inputs in the Juan de Fuca Strait and Eddy Region contribute an amount of (ocean-derived) nitrogen to the Washington shelf comparable to that supplied by local wind-driven upwelling, and an amount to the Vancouver Island shelf clearly greater than that from local wind-driven upwelling.

Lastly, an intriguing result from the regional nitrogen budget in the JDFSER suggests that mass flux deep within the Juan de Fuca canyon seems to be affected by estuarine circulation within the Strait (Figures 12a and 12b). This result deserves further study as it implies a connection between estuarine circulation and flows within the canyon over 40 km offshore of the mouth of the Strait.

Acknowledgments

We would like to thank S. Geier (multiyear moored sensors) and N. Kachel (CTD data) from the ECOHAB-PNW and RISE projects, E. Dever (multiyear moored sensors from the RISE project), R. Thomson (moored arrays and CTD data, Fisheries and Oceans Canada Institute of Ocean Sciences, IOS), B. Peterson (multiyear OR CTD data). Thanks to other members of the PNWTOX and UWCMG groups for useful discussions including M. Foreman, D. *Masson*, S. Lubetkin, R. McCabe, D. Sutherland, C. Bassin, and K. Thyng. D. Darr provided computer cluster administration and support. We would also like to acknowledge that the helpful comments of Jack Barth and another anonymous reviewer significantly improved this manuscript. This work was facilitated through the use of advanced computational, storage, and networking infrastructure provided by the Hyak supercomputer system, supported in part by the University of Washington eScience Institute and was supported by grants from the Coastal Ocean Program of the National Oceanic and Atmospheric Administration (NOAA) (NA09NOS4780180) and the National Science Foundation (NSF) (OCE0942675) as part of the Pacific Northwest Toxins (PNWTOX) project. This is contribution 13 and ECO810 from the PNWTOX and ECOHAB programs, respectively. Observational data from the RISE and ECOHAB PNW programs used for model validation are available through the BCO-DMO repository (http://www.bco-dmo.org/project/2094, http://www.bco-dmo.org/project/2095). NOAA data are available from CDIAC (http://cdiac.ornl.gov). Other observational data can be requested from the aforementioned sources and references cited within the manuscript. Mooring data are available from http://coast.ocean.washington.edu. Model run setup files and output used in this manuscript are available upon request from Parker MacCready (parker@ocean.washington.edu). The statements, findings, conclusions, and recommendations are those of the participants/authors and do not reflect the views of NSF, NOAA or the Department of Commerce.

References

Alford, M. H., and P. MacCready (2014), Flow and mixing in Juan de Fuca Canyon, Washington, *Geophys. Res. Lett.*, *41*, 1608–1615, doi: 10.1002/2013GL058967.

Allen, S. E. (1996), Topographically generated, subinertial flows within a finite length canyon, *J. Phys. Oceanogr.*, *26*, 1608–1632.

Allen, S. E., and B. M. Hickey (2010), Dynamics of advection-driven upwelling over a shelf break submarine canyon, *J. Geophys. Res.*, *115*, C08018, doi:10.1029/2009JC005731.

Allen, S. E., and M. A. Wolfe (2013), Hindcast of the timing of the spring phytoplankton bloom in the Strait of Georgia, 1968–2010, *Prog. Oceanogr.*, *115*, 6–13.

Alvarez-Salgado, X. A., G. Roson, F. F. Perez, F. G. Figueiras, and Y. Pazos (1996), Nitrogen cycling in an estuarine upwelling system, the Ría de Arousa (NW Spain). I: Short-time-scale patterns of hydrodynamics and biogeochemical circulation, *Mar. Ecol. Prog. Ser.*, *135*, 259–273.

Anderson, G. C. (1964), The seasonal and geographic distribution of primary productivity off the Washington and Oregon coasts, *Limnol. Oceanogr.*, *9*(3), 284–302.

Austin, J. A., and J. A. Barth (2002), Variation in the position of the upwelling front on the Oregon shelf, *J. Geophys. Res.*, *107*(C11), 3180, doi: 10.1029/2001JC000858.

Banas, N. S., E. J. Lessard, R. M. Kudela, P. MacCready, T. D. Peterson, B. M. Hickey, and E. Frame (2009a), Planktonic growth and grazing in the Columbia River plume region: A biophysical model study, *J. Geophys. Res.*, *114*, C00B06, doi:10.1029/2008JC004993.

Banas, N. S., P. MacCready, and B. M. Hickey (2009b), The Columbia River plume as along-shelf barrier and cross-shelf exporter: A Lagrangian model study, *Cont. Shelf Res.*, *29*, 292–301.

Barron, C. N., A. B. Kara, P. J. Martin, R. C. Rhodes, and L. F. Smedstad (2006), Formulation, implementation and examination of vertical coordinate choices in the Global Navy Coastal Ocean Model (NCOM), *Ocean Modell.*, *11*, 347–375, doi:10.1016/j.ocemod.2005.01.004.

Bruland, K. W., M. C. Lohan, A. M. Aguilar-Islas, B. S. G. J. Smith, and A. Baptista (2008), Factors influencing the chemistry of the near-field Columbia River plume: Nitrate, silicic acid, dissolved Fe, and dissolved Mn, *J. Geophys. Res.*, *113*, C00B02, doi:10.1029/2007JC004702.

Cannon, G. A. (1972), Wind effects on currents observed in Juan de Fuca Submarine Canyon, *J. Phys. Oceanogr.*, *2*(7), 281–286.

Canuto, V. M., A. Howard, Y. Cheng, and M. S. Dubovikov (2001), Ocean turbulence. Part I: One-point closure model—Momentum and heat vertical diffusivities, *J. Phys. Oceanogr.*, *31*, 1413–1426.

Chase, Z., P. G. Strutton, and B. Hales (2007), Iron links river runoff and shelf width to phytoplankton biomass along the U.S. West Coast, *Geophys. Res. Lett.*, *34*, L04607, doi:10.1029/2006GL028069.

Connolly, T. P., and B. M. Hickey (2014), Regional impact of submarine canyons during seasonal upwelling, *J. Geophys. Res.*, *119*, 953–975, doi:10.1002/2013JC009452.

Crawford, W. R., and R. K. Dewey (1989), Turbulence and mixing: Sources of nutrients on the Vancouver Island continental shelf, *Atmos. Ocean*, *27*(2), 428–442.

Crawford, W. R., and A. Peña (2013), Declining oxygen on the British Columbia continental shelf, *Atmos. Ocean*, *51*(1), 88–103.

Droop, M. (1974), The nutrient status of algal cells in continuous culture, *J. Mar. Biol. Assoc. U. K.*, *54*, 825–855.

Dugdale, R. C. (1967), Nutrient limitation in the sea: Dynamics, identification, and significance, *Limnol. Oceanogr.*, *12*, 685–695.

Dunne, J. P., J. W. Murray, J. Young, L. Balistrieri, and J. K. B. Bishop (1997), 234th and particle cycling in the central equatorial Pacific, *Deep Sea Research II*, *44*, 2049–2083.

Egbert, G. D., and S. Y. Erofeeva (2002), Efficient inverse modeling of barotropic ocean tides, *J. Atmos. Oceanic Technol.*, *19*, 183–204, doi: 10.1175/1520-0426(2002)019<0183:EIMOBO>2.0.CO;2.

Emery, W. J., and R. E. Thomson (2004), *Data Analysis Methods in Physical Oceanography*, 2nd ed., Elsevier, Amsterdam.

Foreman, M. G. G., W. Callendar, A. MacFadyen, B. M. Hickey, R. E. Thomson, and E. D. Lorenzo (2008), Modeling the generation of the Juan de Fuca Eddy, *J. Geophys. Res.*, *113*, C03006, doi:10.1029/2006JC004082.

Frisch, A. S., J. Holbrook, and A. B. Ages (1981), Observations of a summertime reversal in circulation in the Strait of Juan de Fuca, *J. Geophys. Res.*, *86*(C3), 2044–2048.

Giddings, S., P. MacCready, B. Hickey, N. Banas, K. Davis, S. Siedlecki, V. Trainer, R. Kudela, N. Pelland, and T. Connolly (2014), Hindcasts of potential harmful algal bloom transport on the Pacific Northwest coast, *J. Geophys. Res.*, *119*, 2439–2461, doi:10.1002/2013JC009622.

Gotham, I., and G. Rhee (1981), Comparative kinetic studies of nitrate-limited growth and nitrate uptake in phytoplankton in continuous culture, *J. Phycol.*, *17*, 308–314.

Griffin, D. A., and P. H. LeBlond (1990), Estuary/ocean exchange controlled by spring-neap tidal mixing, *Estuarine Coastal Shelf Sci.*, *30*, 275–297.

Groussart, H., and H. Ploug (2001), Microbial degradation of organic carbon and nitrogen on diatom aggregates, *Limnol. Oceanogr.*, *46*(2), 267–277.

Haidvogel, D. B., H. G. Arango, K. Hedstrom, A. Beckmann, P. Malanotte-Rizzoli, and A. F. Shchepetkin (2000), Model evaluation experiments in the North Atlantic Basin: Simulations in nonlinear terrain-following coordinates, *Dyn. Atmos. Oceans*, *32*, 239–281, doi:10.1016/S0377.

Hales, B., J. N. Moum, P. Covert, and A. Perlin (2005), Irreversible nitrate fluxes due to turbulent mixing in a coastal upwelling system, *J. Geophys. Res.*, *110*, C10S11, doi:10.1029/2004JC002685.

Hansen, D. V., and J. Maurice Rattray (1966), New dimensions in estuary classification, *Limnol. Oceanogr.*, *11*(3), 319–326.

Hansen, P. J., P. K. Bjornsen, and B. W. Hansen (1997), Zooplankton grazing and growth: Scaling within the 2-2000 μm body size range, *Limnol. Oceanogr.*, *42*(4), 687–704.

Hartnett, H. E., and A. H. Devol (2003), Role of a strong oxygen-deficient zone in the preservation and degradation of organic matter: A carbon budget for the continental margins of northwest Mexico and Washington State, *Geochim. Cosmochim. Acta*, *67*(2), 247–264.

Herlinveaux, R. H., and J. P. Tully (1961), Some oceanographic features of Juan de Fuca Strait, *J. Fish. Res. Board Can.*, *18*(6), 1027–1071.

Hickey, B., S. Geier, N. Kachel, and A. MacFadyen (2005), A bi-directional river plume: The Columbia in summer, *Cont. Shelf Res.*, *25*, 1631–1656.

Hickey, B., A. MacFadyen, W. Cochlan, R. Kudela, K. Bruland, and C. Trick (2006), Evolution of chemical, biologial, and physical water properties in the northern California Current in 2005: Remote or local wind forcing?, *Geophys. Res. Lett.*, *33*, L22S02, doi:10.1029/2006GL026782.

Hickey, B. M. (1989), Patterns and processes of circulation over the shelf and slope, in *Coastal Oceanography of Washington and Oregon*, edited by B. M. Hickey and M. R. Landry, pp. 41–115, Elsevier Sci., Amsterdam.
Hickey, B. M., and N. S. Banas (2008), Why is the northern end of the California Current System so productive?, *Oceanography*, *21*(4), 90–107.
Hickey, B. M., R. E. Thomson, H. Yih, and P. H. LeBlond (1991), Velocity and temperature fluctuations in a buoyancy-driven current off Vancouver Island, *J. Geophys. Res.*, *96*(C6), 10,507–10,538.
Hickey, B. M., X. Zhang, and N. Banas (2002), Baroclinic coupling between an eastern boundary ocean and a flood plain estuary (Willapa Bay) during low riverflow, summer conditions, *J. Geophys. Res.*, *107*(C10), 3166, doi:10.1029/1999JC000160.
Hickey, B. M., R. McCabe, R. M. Kudela, E. P. Dever, and S. Geier (2009), Three interacting freshwater plumes in the northern California Current System, *J. Geophys. Res.*, *114*, C00B03, doi:10.1029/2008JC004907.
Hickey, B. M., et al. (2010), River influences on shelf ecosystems: Introduction and synthesis, *J. Geophys. Res.*, *115*, C00B17, doi:10.1029/2009JC005452.
Holbrook, J. R., and D. Halpern (1982), Winter-time near-surface currents in the Strait of Juan de Fuca, *Atmos. Ocean*, *20*(4), 327–339.
Holbrook, J. R., R. D. Muench, D. G. Kachel, and C. Wright (1980), Circulation in the Strait of Juan de Fuca: Recent oceanographic observations in the eastern basin, *NOAA Tech. Rep. PMEL*, *33*, 42 pp.
Huyer, A. (1983), Coastal upwelling in the California Current system, *Prog. Oceanogr.*, *12*, 259–284.
Johannessen, S. C., R. W. Macdonald, and D. W. Paton (2003), A sediment and organic carbon budget for the greater Strait of Georgia, *Estuarine Coastal Shelf Sci.*, *56*, 845–860, doi:10.1016/s0272-7714(02)00303-7.
Khangaonkar, T., B. Sackmann, W. Long, T. Mohamedali, and M. Roberts (2012), Simulation of annual biogeochemical cycles of nutrient balance, phytoplankton bloom(s), and DO in Puget Sound using an unstructured grid model, *Ocean Dyn.*, *62*, 1353–1379.
Kosro, P. M., W. T. Peterson, B. M. Hickey, R. K. Shearman, and S. D. Pierce (2006), Physical versus biological spring transition: 2005, *Geophys. Res. Lett.*, *33*, L22S03, doi:10.1029/2006GL027072.
Kudela, R. M., and T. D. Peterson (2009), Influence of a buoyant river plume on phytoplankton nutrient dynamics: What controls standing stocks and productivity?, *J. Geophys. Res.*, *114*, C00B11, doi:10.1029/2008JC004913.
Kudela, R. M., W. P. Cochlan, T. D. Peterson, and C. G. Trick (2006), Impacts on phytoplankton biomass and productivity in the Pacific Northwest during the warm ocean conditions of 2005, *Geophys. Res. Lett.*, *33*, L22S06, doi:10.1029/2006GL026772.
Kudela, R. M., et al. (2010), Multiple trophic levels fueled by circulation in the Columbia River plume, *Geophys. Res. Lett.*, *37*, L18607, doi:10.1029/2010GL044342.
Lohan, M. C., and K. W. Bruland (2006), Importance of vertical mixing for additional sources of nitrate and iron to surface waters of the Columbia River plume: Implications for biology, *Mar. Chem.*, *98*, 260–273, doi:10.1016/j.marchem.2005.10.003.
MacCready, P., N. S. Banas, B. M. Hickey, E. P. Dever, and Y. Liu (2009), A model study of tide- and wind-induced mixing in the Columbia River Estuary and plume, *Cont. Shelf Res.*, *29*(1), 278–291.
MacFadyen, A., and B. M. Hickey (2010), Generation and evolution of a topographically linked, mesoscale eddy under steady and variabile wind-forcing, *Cont. Shelf Res.*, *30*, 1387–1402.
MacFadyen, A., B. M. Hickey, and M. G. G. Foreman (2005), Transport of surface waters from the Juan de Fuca eddy region to the Washington coast, *Cont. Shelf Res.*, *25*, 2008–2021, doi:10.1016/j.csr.2005.07.005.
MacFadyen, A., B. M. Hickey, and W. P. Cochlan (2008), Influences of the Juan de Fuca Eddy on circulation, nutrients, and phytoplankton production in the northern California Current System, *J. Geophys. Res.*, *113*, C08008, doi:10.1029/2007JC004412.
Mackas, D. L., and P. J. Harrison (1997), Nitrogenous nutrient sources and sinks in the Juan de Fuca Strait/Strait of Georgia/Puget Sound Estuarient System: Assesing the Potential for Eutrophication, *Estuarine Coastal Shelf Sci.*, *44*(1), 1–21.
Mackas, D. L., G. C. Louttit, and M. J. Austin (1980), Spatial distribution of zooplankton and phytoplankton in British Columbian coastal waters, *Can. J. Aquat. Sci.*, *37*, 1476–1487.
Mackas, D. L., W. T. Peterson, M. D. Ohman, and B. E. Lavaniegos (2006), Zooplankton anomalies in the California Current system before and during the warm ocean conditions of 2005, *Geophys. Res. Lett.*, *33*, L22S07, doi:10.1029/2006GL027930.
Mass, C. F., et al. (2003), Regional environmental prediction over the Pacific Northwest, *Bull. Am. Meteorol. Soc.*, *84*, 1353–1366, doi:10.1175/BAMS-84-10-1353.
Masson, D. (2006), Seasonal water mass analysis for the Straits of Juan de Fuca and Georgia, *Atmos. Ocean*, *44*(1), 1–15.
Masson, D., and P. F. Cummins (2004), Observations and modeling of seasonal variability in the Straits of Georgia and Juan de Fuca, *J. Mar. Res.*, *62*, 491–516.
Masson, D., and A. Peña (2009), Chlorophyll distribution in a temperate estuary: The Strait of Georgia and Juan de Fuca Strait, *Estuarine Coastal Shelf Sci.*, *82*, 19–28.
Monteiro, P. M. S., and J. L. Largier (1999), Thermal stratification in Saldanha Bay (South Africa) and subtidal, density-driven exchange with the coastal waters of the Benjuela Upwelling System, *Estuarine Coastal Shelf Sci.*, *49*(6), 877–890.
Orton, P. M., and D. A. Jay (2005), Observations at the tidal plume front of a high-volume river outflow, *Geophys. Res. Lett.*, *32*, L11605, doi:10.1029/2005GL022372.
Siedlecki, S., N. Banas, K. Davis, S. Giddings. B. Hickey, P. MacCready, T. Connolly, and S. Geier (2014), Seasonal and interannual oxygen variability on the Washington and Oregon continental shelves, *J. Geophys. Res. Oceans*, doi:10.1002/2014JC010254, in press.
Small, L., and D. W. Menzies (1981), Patterns of primary productivity and biomass in a coastal upwelling region, *Deep Sea Res., Part A*, *28*, 123–149.
Smith, R. L. (1974), A description of current, wind and sea level variations during coastal upwelling off the Oregon coast, July-August 1972, *J. Geophys. Res.*, *79*, 435–443.
Smith, S. L., Y. Yamanaka, M. Pahlow, and A. Oschlies (2009), Optimal uptake kinetics: Physiological acclimation explains the pattern of nitrate uptake by phytoplankton in the ocean, *Mar. Ecol. Prog. Ser.*, *384*, 1–12.
Stow, C. A., J. Jolliff, J. Dennis J. McGillicuddy, S. C. Doney, J. I. Allen, M. A. M. Friedrichs, K. A. Rose, and P. Wallhead (2009), Skill assessment for coupled biological/physical models of marine systems, *J. Mar. Syst.*, *76*, 4–15.
Strub, P. T., P. M. Kosro, and A. Huyer (1991), The nature of cold filaments in the California Current system, *J. Geophys. Res.*, *96*(C8), 14,743–14,768.
Sutherland, D. A., P. MacCready, N. S. Banas, and L. F. Smedstad (2011), A model study of the Salish Sea Estuarine Circulation, *J. Phys. Oceanogr.*, *41*, 1125–1143, doi:10.1175/2011JPO4540.1.
Sutton, J. N., S. C. Johannessen, and R. W. Macdonald (2013), A nitrogen budget for the Strait of Georgia, British Columbia, *Biogeosci. Discuss.*, *10*, 7135–7169, doi:10.5194/bgd-10-7135-2013.
Sydeman, W. J., R. W. Bradley, P. Warzybok, C. L. Abraham, J. Jahncke, K. D. Hyrenbach, V. Kousky, J. M. Hipfner, and M. D. Ohman (2006), Planktivorous auklet Ptychoramphus aleuticus responses to ocean climate, 2005: Unusual atmospheric blocking?, *Geophys. Res. Lett.*, *33*, L22S09, doi:10.1029/2006GL026736.

Thomas, A. C., and P. Brickley (2006), Satellite measurements of chlorophyll distribution during spring 2005 in the California Current, *Geophys. Res. Lett.*, *33*, L22S09, doi:10.1029/2006GL026736.

Thomson, R. E., S. F. Mihály, and E. A. Kulikov (2007), Estuarine versus transient flow regimes in Juan de Fuca Strait, *J. Geophys. Res.*, *112*, C09022, doi:10.1029/2006JC003925.

Trainer, V. L., B. M. Hickey, W. P. Cochlan, E. J. Lessard, C. G. Trick, M. L. Wells, J. Herndon, A. MacFadyen, and S. K. Moore (2009), Seasonal and interannual variability of Pseudo-nitzschia and domoic acid in the Juan de Fuca Eddy region and its adjacent shelves, *Limnol. Oceanogr. Methods*, *54*(1), 289–308.

Umlauf, L., and H. Burchard (2003), A generic length-scale equation for geophysical turbulence models, *J. Mar. Res.*, *61*, 235–265.

Waldichuk, M. (1957), Physical oceanography of the Strait of Georgia, British Columbia, *J. Fish. Res. Board Can.*, *14*, 321–486.

Ware, D. M., and R. E. Thomson (2005), Bottom-up ecosystem trophic dynamics determine fish production in the northeastern Pacific, *Science*, *308*, 1280–1284.

Wetz, M. S., B. Hales, Z. Chase, P. A. Wheeler, and M. M. Whitney (2006), Riverine input of macronutrients, iron, and organic matter to the coastal ocean off Oregon, U.S.A., during the winter, *Limnol. Oceanogr. Methods*, *51*(5), 2221–2231.

Willmott, C. J. (1982), Some comments on the evaluation of model performance, *Bull. Am. Meteorol. Soc.*, *63*, 1309–1313.

WOCE Data Products Committee (2002), WOCE Global Data, Version 3.0, *Rep. 180/02*, WOCE Int. Project Off., Southampton, U. K.